Fall 12-16-2023

Main Effects Screening Study of Fe/KClO4 Thermal Battery Heat Pellet Resistive Activation

Bryan T. Steiner

Bryan T. Steiner
Candidate

Mechanical Engineering
Department

This thesis is approved, and it is acceptable in quality and form for publication:

Approved by the Thesis Committee:

Peter Vorobieff , Chairperson

Henry Padilla

Pankaj Kumar

MAIN EFFECTS SCREENING STUDY OF FE/KCLO4 THERMAL BATTERY HEAT PELLET RESISTIVE ACTIVATION

by

BRYAN T. STEINER

B.S., MECHANICAL ENGINEERING, UNIVERSITY OF NEW MEXICO, 2020

THESIS

Submitted in Partial Fulfillment of the
Requirements for the Degree of

Master of Science
Mechanical Engineering

The University of New Mexico
Albuquerque, New Mexico

December, 2023

ACKNOWLEDGMENTS

I would like to acknowledge and thank the many people who have contributed towards this work. I am deeply grateful to my chair and professor Dr. Vorobieff for his direction, feedback, and patience as this project has progressed, as well as the academic instruction I have greatly benefited from. I am also very thankful for the extremely valuable advice and direction from Henry Padilla and Janet Leavitt. Dr. Kumar's involvement in the thesis committee is much appreciated. I am very grateful to Bob Fox, Alan Harrington, Bertha Montoya, and Louie Cano for their excellent work in making these experiments possible.

Sandia National Laboratories is a multimission laboratory managed and operated by National Technology & Engineering Solutions of Sandia, LLC, a wholly owned subsidiary of Honeywell International Inc., for the U.S. Department of Energy's National Nuclear Security Administration under contract DE-NA0003525.

This paper describes objective technical results and analysis. Any subjective views or opinions that might be expressed in the paper do not necessarily represent the views of the U.S. Department of Energy or the United States Government.

Main Effects Screening of Fe/KCIO4 Thermal
Battery Heat Restrictive Activation

B.S., Mechanical Engineering, University of New Mexico, 2023
M.S., Mechanical Engineering, University of New Mexico, 2023

ABSTRACT

Thermal battery iron-potassium perchlorate ($Fe/KClO_4$) heat pellets are often ignited by explosive igniters or heat paper. An alternative direct electrical ignition method via resistive heating is explored, which could improve thermal battery manufacturability and design flexibility. A main effects screening experiment was performed with the goal of confirming prior observed trends under more realistic test conditions and ranking the importance of design factors, to optimize future experiments and develop knowledge of the performance space. Relevant literature is examined to advance a theoretical understanding of resistive activation. Ignition sensitivity (go/no-go and time to ignition) and ignition energy are primary responses that determine the feasibility of this technology in thermal batteries. Heat pellet density, electrode gap size, ignition circuit line resistance and voltage, and iron particle size are important factors that influence these responses. With this information, future experiments can be optimized because the design tradespace for resistive activation is better understood.

Table of Contents

List of Figures

List of Tables

Chapter 1. Introduction and background

1.1 Overview

Thermally activated batteries, henceforth referred to as thermal batteries, are often used in applications where long shelf life, high reliability, resilience in mechanically challenging environments, and high power density are required. These thermal batteries are not to be confused with thermal storage batteries, which is a device that stores thermal energy. Rather, thermally activated batteries are electrical batteries that have solid, nonconductive electrolyte at room temperature. A heat source that can provide temperatures of up to 550°C is required to melt the electrolyte and activate the battery. These power sources are often found in missile systems, ordnance, and other military applications such as emergency backup aircraft power (Guidotti & Masset, 2006). An additional application is in geothermal boreholes, where the use of a battery design that can withstand high temperatures is desired (Niu et al., 2014). Conventional thermal battery designs take the shape of a cylindrical stack of cells. The amount of cells varies depending on the system requirements. Electrochemistry has changed over time, but modern designs have mostly settled on two options: Li/FeS2 and Li/CoS2. Compared to earlier designs using Ca/CaCrO4, these newer designs are less toxic and provide power, runtime, and reliability advantages. The earliest thermal batteries were used in German rockets during World War II, where the waste heat from the rocket motor produced the heat required to run the battery (Guidotti, 1995). Subsequent designs with internal heat generation used only the $Zr/BaCrO_4$ heat paper. However, research into pelletized heat sources was conducted on behalf of Sandia in 1970 by Unidynamics/Phoenix and the technology was adopted for future use (Rittenhouse, 1970). Current battery designs use these heat pellets to generate their heat internally. Heat pellets are made of mixed iron-

potassium perchlorate powder pressed into a flat disk shape under high force using 40-ton presses.

Thermal batteries have two main configurations: center-fired and side-fired. In side-fired batteries, an igniter fires the first heat pellet in the stack. This in turn ignites a heat paper fuse strip made from $Zr/BaCrO_4$ that runs down the side of the stack, extending the ignition train to the heat pellet in each cell. Center-fired batteries have an axially-centered hole through the entire battery stack, with heat pellets sandwiching each cell. An igniter sends hot particles down the center hole, igniting each heat pellet upon contact and activating each cell. These batteries have lower energy density than side fired batteries because of the axial hole through each cell. Batteries designed for longer runtime typically include insulation wrapping the cell stack and on its top and bottom. Batteries often use a steel casing, with glass-to-metal seals allowing connections to the cells from outside the battery, while preserving hermeticity. (Visvaldis & Charles, 2002, pp. 21-1 – 21-6)

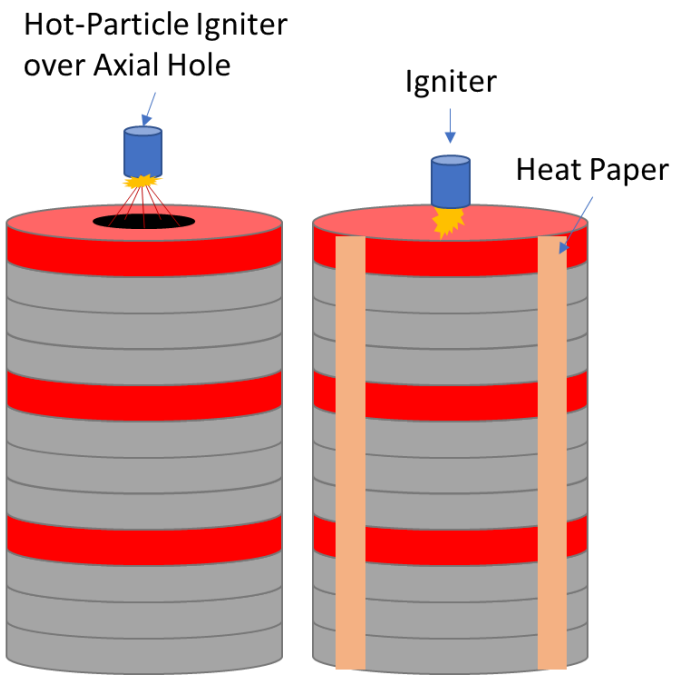

Figure 1. Typical center-fired (left) and side-fired (right) thermal battery configurations. Red discs represent heat pellets in the cell stack. Note that the axial hole for the center-fired battery is through the entire stack.

To manufacture heat pellets, the iron and potassium perchlorate powders are sieved and blended before pressing to ensure small uniform particle sizes and good mixing. Ignitability is an important consideration, as well as how the mixture holds together after being pressed. The stoichiometric ratio for the ignition reaction is around 62% weight percent Fe, but heat pellets typically have a much higher iron content, of around 82-88%. This is because the pellet must maintain its original shape to provide mechanical support for the rest of the battery stack, and to provide a conductive path for the power generated by the cell. Another consideration for this chemistry is that the pellet must also burn quickly, so that the battery may respond promptly after the ignition signal (Guidotti et al., 2006)

While current thermal battery designs are reliable, have long shelf lives, and meet the requirements of the systems they are used in, there is still room to improve their designs. The Zr/$BaCrO_4$ heat paper is toxic and presents hazards to workers involved in manufacturing

and disassembling thermal batteries, and an alternate initiation technology has the potential to replace heat paper as well as igniters. Manufacturing complexity in terms of assembly and supply chain could be simplified, and replacing igniters would cause thermal battery volume to be decreased. To replace just the igniter, only the first heat pellet in a side-fired battery would need to activate. To totally replace heat paper in side-fired batteries, each heat pellet would need to be fired independently, but this could result in a faster rise time. This may also result in more consistent battery rise times due to less variability from heat paper.

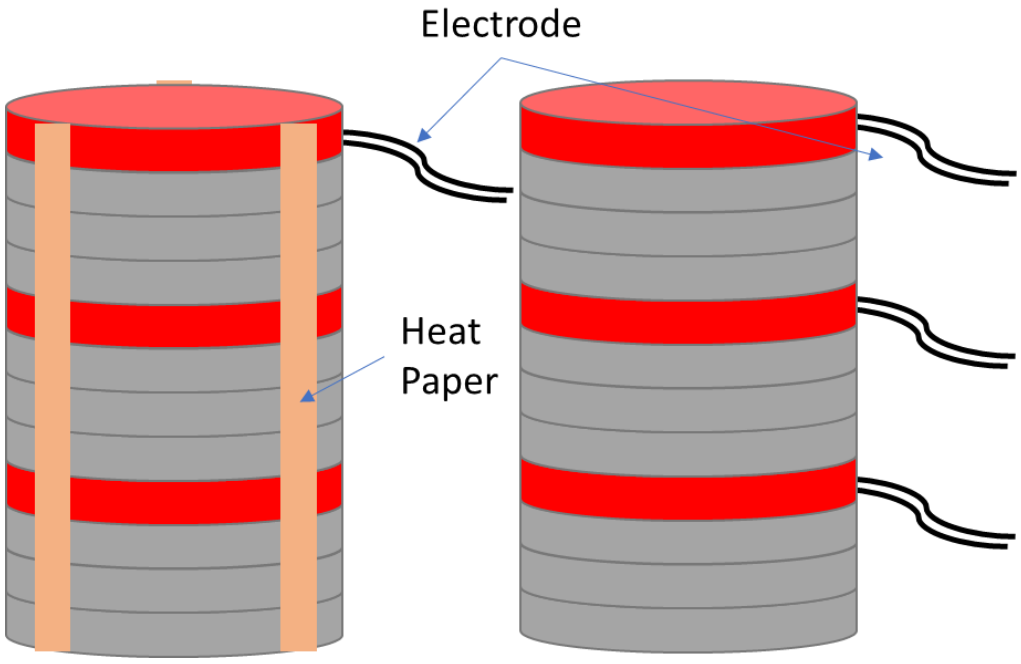

Figure 2. Comparison of single (right) vs multi electrode (left) configurations with resistive activation technology. Red discs represent the heat pellets in the cell stack.

The alternative initiation technology that is considered in this work is known as resistive activation. Instead of an igniter, electrodes contact the heat pellet and pass current through the iron matrix of the powder. The resistance in this conductive path raises the temperature of the path through the mechanism of joule heating. If the temperature reaches a critical level,

the combustion reaction will start. This must happen quickly to prevent quenching of burning, as heat can transfer away from the critical volume between the electrodes too rapidly. Many different variables have effects on this process.

1.2 Project Background

In 2020, a study at SNL (Sandia National Laboratories) was performed to determine the effect of some variables on resistive activation, as well as to ascertain the feasibility of the technology in production thermal batteries (Padilla, 2020). Over 180 tests, three different factors were studied: stoichiometry ratio, density, and electrode spacing.

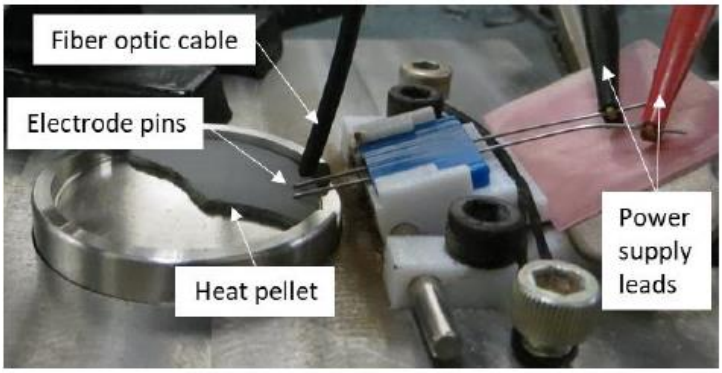

Figure 3. Experimental fixture from 2020 study (Padilla, 2020). A pellet fragment is loaded in the fixture, itself normally mounted inside a boombox during the duration of a test. Hastelloy electrode pins with hemispherical ends are pressed against the top surface of a heat pellet. A fiber optic cable points between the pin tips and records the intensity of light emitted so that time of ignition can be determined precisely.

For the resistive activation technology to be a feasible replacement for the igniters used in thermal batteries, similar power requirements and ignition times are needed. This initial study showed that these requirements could be met, and that further development work was warranted. The main takeaways from the study were that a lower electrode gap size would cause consistently faster ignitions and that lower iron powder content required less energy and more time to ignite than more fuel-rich ratios. Similarly, pellets with lower pressing density required less energy and more time to ignite than their denser counterparts. Statistical

analysis in the JMP software (2021) concluded that each variable, and their interactions, had a statistically significant impact on the responses of ignition time and ignition power.

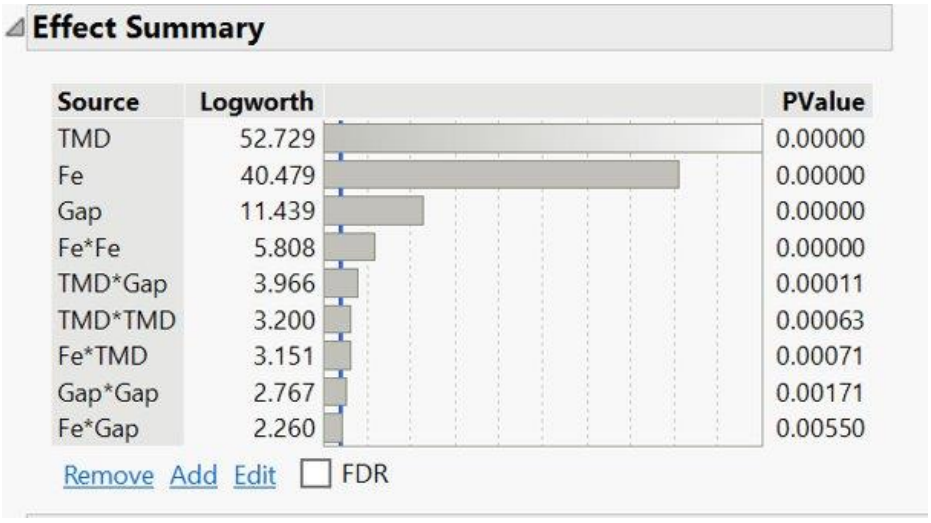

Figure 4. JMP summary of effects for 2020 study

One batch of powder used in the 2020 work had a significantly smaller average particle size than the others. Data from this batch was not consistent with the trends of the other batches, since particle size was not intended to be a variable in testing. However, this batch had improved ignition characteristics compared to the others, providing a reason to look at particle size in future experiments.

Therefore, the next step in the experimental work performed at SNL focused on particle size. Two different Fe particle sizes were evaluated: 16 and 32 microns average (D50) size. The powder with the smaller size ignited faster, with less energy required, and less variance in ignition time and energy than the larger iron size powder.

After this, the effect of lower iron/oxidizer ratios was examined. Previously, the lowest iron/oxidizer weight ratio examined was 82/18%, while the stoichiometric ratio is 61.8/38.2%. 70%, 75%, and 80% iron content pellets were pressed and tested using the same

ignition fixture and experimental setup as before. While lower iron contents ignited more easily, the 70% and 75% formulations tended to melt. Since the heat pellet needs to maintain its shape inside the thermal battery to provide a conductive pathway for the cells and support for the battery stack, formulations below 80% iron are not useful. 80% may be useful, but further testing may be required to determine if it works well under compression.

After these experiments were completed, work to develop internal electrode designs commenced. These electrodes were needed to test the performance of resistive activation under compression, and to start the design process for integrating into a battery.

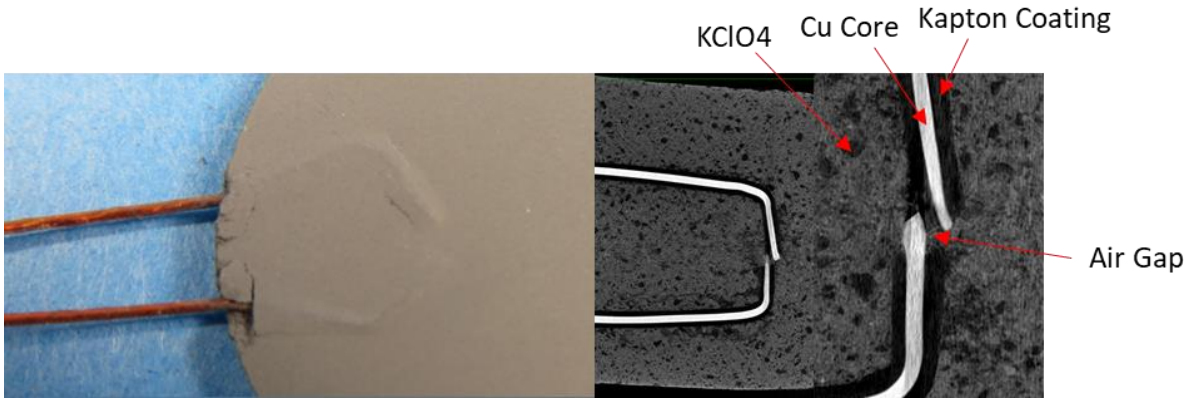

Figure 5. Heat pellet with Kapton insulated silver-coated copper wires embedded, and CT scan of open-resistance pellet with misaligned electrodes.

Manufacturing pellets with internal electrodes proved to be a challenge. Often, with the first prototypes, the electrode tips were not aligned well within the pellet. A computerized tomography scan of a pellet reading open resistance was taken, showing a possible air gap within the pellet. It was theorized that the Poisson effect could open an air gap inside the pellet under compression since just the end of the wire was exposed. This indicated that further work had to be done to develop the electrode design.

Nevertheless, experiments were performed to assess how changes in wire gauge, wire tip orientation, and exposed electrode contact area affected ignition. A smaller contact area and opposing tip orientation produced faster and lower power ignitions.

For the reasons discussed above, a different wire design was chosen for further testing. This consisted of a 34-gauge (0.0063”, 0.16002mm diameter) Kapton-coated wire wrapped around a mandrel, then twisted together (see Figure 6. Twisted wire assembly after cutting. This resulted in a twisted wire with a continuous loop at one end, which was then cut with a razor blade to produce two electrodes. This design presents several advantages. First, the electrodes stay aligned through the pressing process much more easily because they are twisted together. Second, the gap size can be precisely controlled. Another way that the design was improved was to remove the Kapton on one or both faces of the loop. This would ensure that the electrodes would maintain contact under compression, since the area of the conductor that was exposed would be normal to the compression axis. This design of electrode proved to be much easier to manufacture, and to have much more consistent resistance measurements between pellets. Kapton was removed from the wires by either scraping with a razor blade or by a laser welder.

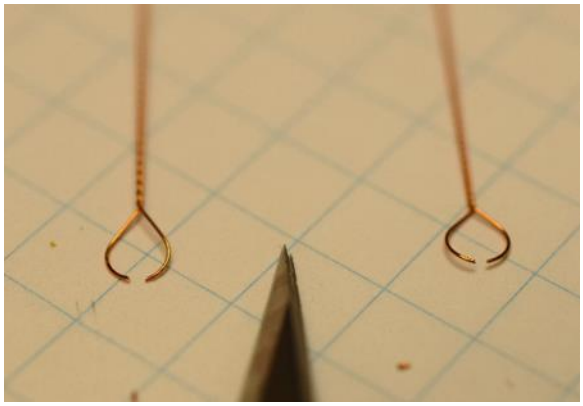

Figure 6. Twisted wire assembly after cutting.

The ignition response was evaluated for these “second generation” electrodes in a small experiment. Different contact areas and ways of removing Kapton were evaluated. First, resistance measurements were taken of each pellet to determine the relationship between resistance and contact area for each method of removing Kapton. Then, ignition testing was performed on these pellets.

The conclusion from this experiment was that laser ablation is the superior method of controlling contact area, since the ignition results were much better. However, there was some variability in the resistance measurements pre-test, so more work would be required to improve the laser ablation process. One other aspect of the design that was noted is that larger contact areas provided more consistent contact during the test. This can be seen in the difference between the oscilloscope waveforms for the different groups of wires. Since this data is used to calculate dynamic resistance, power, and cumulative energy, non-noisy waveforms are ideal.

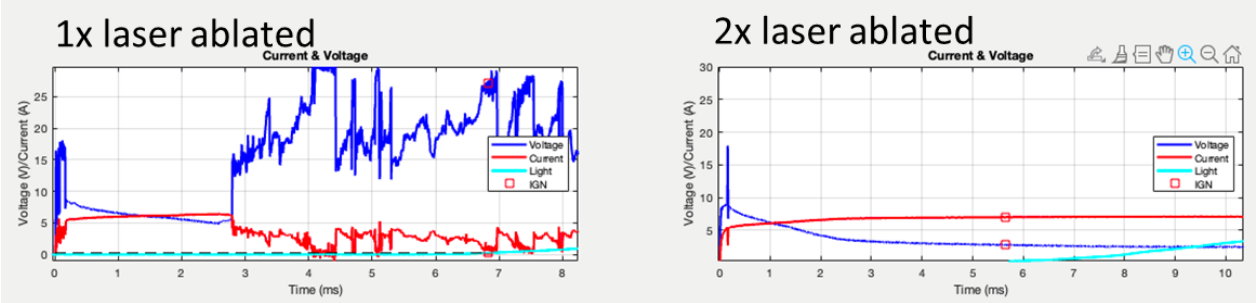

Figure 7. Difference between waveform results for different contact areas.

To get more consistent and repeatable contact areas, it was necessary to determine laser welder power settings that caused Kapton to ablate without the copper melting (See Table 1. Experimentation to determine ideal energy settings for electrode Kapton ablation and Figure 8. Energy values for laser ablation corresponding to Table 1. After some experimentation, an

energy setting of 0.405 Joules was found to give the best results (See Figure 9). The electrodes used in the experiments that are the focus of this thesis are made in this way.

Table 1. Experimentation to determine ideal energy settings for electrode Kapton ablation

#	Power (kW)	Time (ms)	Energy (J)	# Times hit	Energy x # times hit	Result
1	0.2	3	0.6	2	1.2	Melted copper
2	0.15	3	0.45	2	0.9	Melted copper
3	0.15	1.5	0.225	2	0.45	Kapton not burned off fully
4	0.15	2	0.3	2	0.6	Better Kapton removal but not fully complete
5	0.17	2	0.34	2	0.68	Kapton not burned off fully
6	0.17	2	0.34	3	1.02	Hit top/bottom/top, Kapton was ablated away with some carbon remaining, copper not melted
7	0.17	2	0.34	2	0.68	Kapton not burned off fully

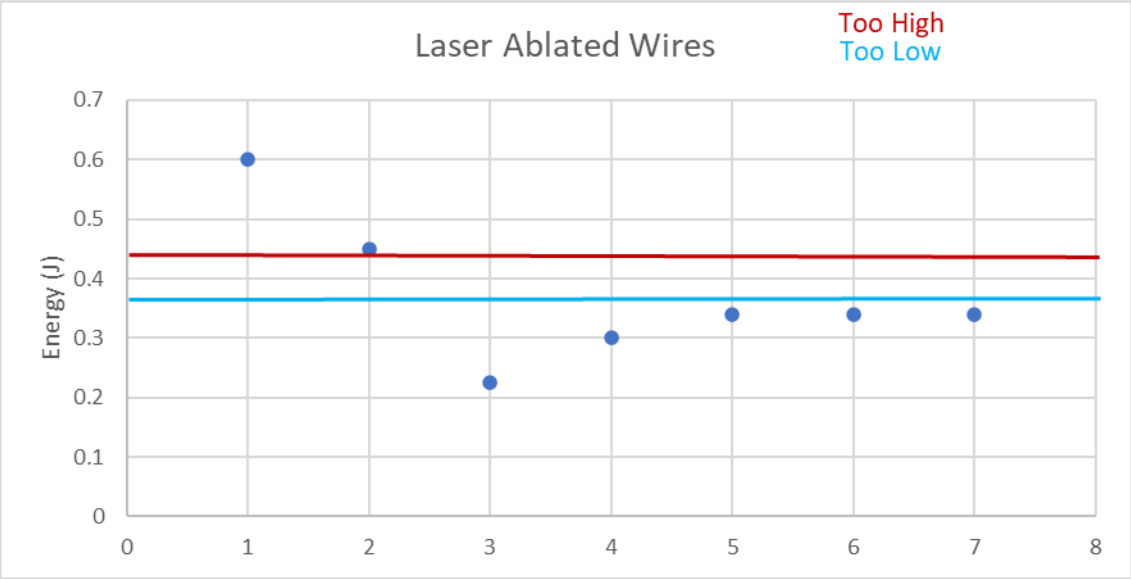

Figure 8. Energy values for laser ablation corresponding to Table 1

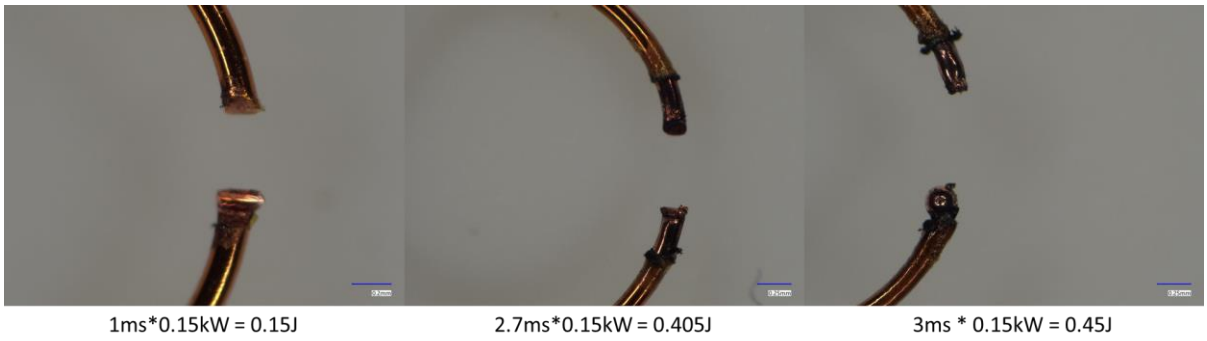

Figure 9. Laser ablated electrodes showing the differences between energy levels.

For future development work, flexible printed circuit electrodes will be designed, built, and tested. These are external to the pellet and will most likely closely represent the final design that could be integrated into production thermal batteries. The basic design is a copper conductor sandwiched between two layers of Kapton. Even though there are differences between the designs, conclusions from testing different internal electrode configurations will

provide useful insight into the design of external flexible printed circuit electrodes. These new electrodes will be under compression and have similar contact area and dimensions as the internal designs.

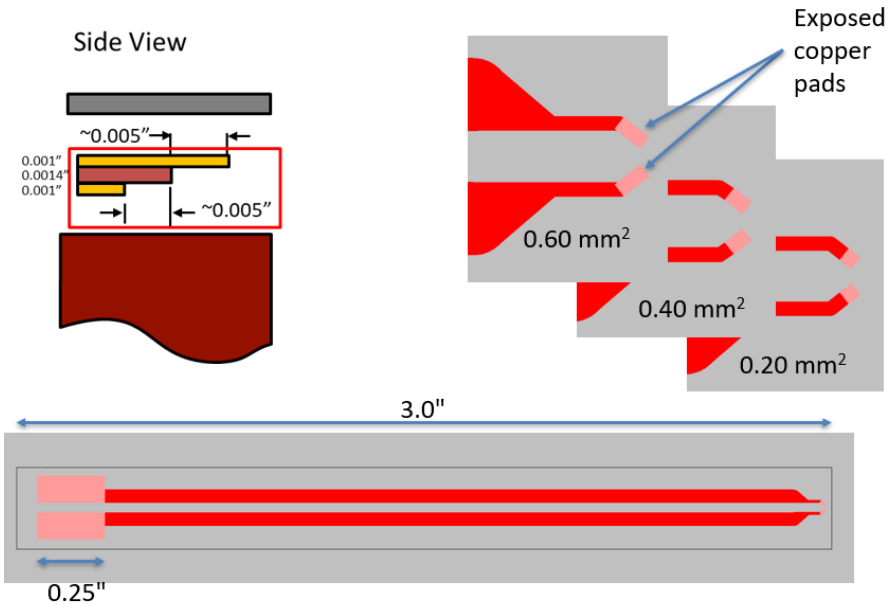

Figure 10. External flexible printed circuit electrodes.

The work before the current project that focused on heat pellets in thermal battery applications has generally not considered electrical ignition as a topic of study. However, many of the characterization studies and prior work done is applicable and provides helpful insights into designing the experimental space.

1.3 Prior work

To examine the available literature regarding the physics of heat powder, multiple articles will be discussed. One of the first documents that has direct application to resistive activation is a Unidynamics (Rittenhouse, 1970) study that characterized heat pellets in an effort to develop the technology for use in thermal batteries for the first time. In this work, factors were investigated to determine their effect on ignition sensitivity and pellet strength. Of

particular relevance to this thesis is Rittenhouse's description of the ignition testing experiments and the relationship between density and ignition sensitivity. For this testing setup, capacitors were used to produce an arc between two electrodes, which could be visualized due to the flow of argon gas. Various capacitor sizes could be selected to change the amount of power discharged. Data was collected showing an effect of pellet density on ignition sensitivity. Densities ranging from 3.3 to 3.7 g/cm^3 were evaluated with 0.1 gm/cm^3 intervals. The data collected showed that less dense pellets tended to require less energy to fire. Also, powder blends with smaller $KClO_4$ particles were more likely to ignite than those with larger particles.

An article by Guidotti et al. (2006) presented background information on thermal battery and heat pellet technology, along with work to further characterize heat powder and pellets. Different commercial sources of Fe powder were characterized. The experimental parameters included forming pressure, pellet break strength, purity of the Fe powder, calorific output, burn rate, peak temperatures, and ignition sensitivity. In addition to comparing different commercial Fe sources, stoichiometric ratio, pressing density, and particle size were the parameters that were varied during the experiments. For the resistive activation project, the data concerning ignition sensitivity is of interest, although a laser was used to initiate combustion. For the pressing densities used in the experiments, ignition sensitivity increased with density. This appears to be contrary to some of the other work mentioned in this literature review. This work also concluded that more energy was required to ignite pellets with larger particle sizes and lower potassium perchlorate content. The authors concluded that density was the most important factor for ignition sensitivity, along with the type of iron powder used. The results of this study suggest that heat pellets with higher densities, lower

particle sizes, and higher potassium perchlorate content would be more desirable for resistive activation purposes.

An early paper, prepared by T. P. Evans (1984), documented ignition sensitivity testing on several different batches of heat powder. The powder was pressed into pellets of various density levels and tested using a capacitor discharge device with sewing-pin electrodes. To determine ignition sensitivity, a stepping function with increments of 1 volt was used, with the pellet rotated so that a fresh surface could be exposed to the electrodes between each step. The batches of powder tested included two different lots of 88/12 powder and one lot of 84/16 powder. The results of testing showed considerable differences between batches, in terms of the energy required for ignition. Ignition versus density sensitivity curves were similar shape for the different batches, all concave up with a minimum somewhere between 3 and 4 grams/cm^3. Beyond 3.8 grams/cm^3 (64.6% TMD for 84/16 stoichiometry, and 60.5% TMD for 88/12), energy required for ignition rises drastically. Over 4.8 grams/cm^3 (81.6% TMD for 84/16, and 76.4% TMD for 88/12), the capacitor discharge device was not able to initiate combustion. The author speculates that the forces required to press to 4.8 grams/cm^3 deform iron particles in a way that inhibits the pyrotechnic reaction. This paper shows that density is a very important factor in ignition sensitivity. Even though heat pellets are ignited in a different way in the TBRA (Thermal Battery Resistive Activation) project, their sensitivity to ignition appears to follow a very similar trend. Pellets have not been pressed and tested with densities as high as described in Evan's report, so an upper range on pressing density is useful to design efficient experiments.

The paper by Cooper et al. (2021) presents research into the electrical conduction properties of compressed two-material powder mixtures where one powder is a porous, sponge-like

electrical conductor. This type of mixture is that of thermal battery heat powder. Finite element modeling was performed to study the effect of powder geometry on the percolation threshold, below which a conductive path does not exist in a randomly populated matrix. Specifically, the variables changed were particle size and number of contacts between particles. In this model, a voltage differential was introduced across the cubic mesh, and the resulting electrical currents were recorded. The percolation threshold was determined based on whether these currents connected across opposing surfaces in the volume. The results of the study clearly showed that differing particle arrangements had large effects on the percolation threshold and conductivity. Also, larger metal volume fractions were correlated with higher conductivity and lower percolation thresholds. In addition to finite element modeling, physical experiments were performed. The materials used were titanium and potassium perchlorate, and iron and potassium perchlorate. Electrical resistance measurements were taken while the powder was being compressed with increasing force. An optical sensor was used to track the position of the rams. This enabled the volume of the powder sample to be measured for the purpose of calculating conductivity as pressure varied with time. Relative density was also calculated using the volume measurements and known maximum density values for the constituent materials. Relative density (in terms of percentage of theoretical maximum density) is considered to be more important than absolute density because the absolute density depends on the weight ratio of iron and potassium perchlorate, but using relative density makes comparison between different weight ratio powder batches easier. When conductivity was plotted vs relative density, a logarithm function shape was clearly observed. This showed that conductivity increased rapidly for smaller changes at low relative density. Conductivity then increased slowly, as if

approaching an asymptote, for changes at higher relative density. When a plot is made of relative density vs. applied stress with a log axis for applied stress, there is a point before which the curve is linear and shallow. After this point, it shifts to a fairly linear but significantly steeper curve. This point is likely where the powder changes from a rearrangement to deformation regime. For the iron mixtures examined, this happened where the density was around 36% of the maximum theoretical density. Notably, this inflection point also appears in the conductivity/relative density plot, where the conductivity starts to increase slower with increases in relative density.

Abdelmoneim's (2010) article explores the temperature to conductivity relationship for potassium perchlorate, as well as the relationship between conductivity and frequency of the applied alternating current. For resistive activation, the conductivity of potassium perchlorate is important for the overall conduction of the heat pellet. While potassium perchlorate is usually understood to be an insulator, its conductivity is dependent on temperature. As current flows into the pellet, one would expect the conductance to increase over time as the iron particle connections between the electrodes heat up and eventually start to melt the potassium perchlorate. Three distinct regions in the relation of conductivity and temperature were observed. The first region, between 300°K and 480°K, shows that conductivity does not change much with temperature. Between 480°K and 575°K, the conductivity increases with temperature much more significantly. Past 575°K, conductivity increases with temperature at a shallower rate. This data shows that, around 480°K, the expected resistance of a pellet would drop significantly. This would occur from resistance heating in the iron matrix and would possibly explain the drop in resistance seen in the first few milliseconds of the ignition signal.

An article by Lee (2015) covers the mechanics of thermal conduction in a two-material mixture. In addition to electrical conduction, thermal conduction is an important factor that influences ignition for heat pellets. Starting the combustion reaction requires there to be a volume of heat powder that reaches a critical temperature. If the powder is too thermally conductive, it may take longer than desired to reach this critical temperature. Since the powder is a mixture of two materials, it is complicated to analyze thermal conduction. One factor in this is the particle size of each material, in addition to the ratio of mixtures and the density. This article analyzes one of these factors for the case of shredded rubber tire particles in a glass matrix, which represents an important material for civil engineering purposes. However, the conclusions should be applicable to the purposes of the resistive activation project because of the similarities of the mixtures. Experiments were performed comparing the thermal conduction of different mixtures of glass beads and rubber particles, sand and rubber particles, and electrical conduction of different glass bead/chrome ball mixtures to determine the effect of particle contact. Computer modeling was also performed. The study concluded that smaller insulating particles are correlated with decreased thermal conductivity, because they can interrupt the conducting pathways of the other material. Also, decreasing the volume fraction of insulator to conductor material increases thermal conductivity. This appears to have a larger impact on conductivity than the size ratio. For minimizing the energy required for heat pellet ignition, this would seem to indicate that small insulating potassium perchlorate particles are more desirable. Compared to the large range of insulator/conductor ratios in the article, however, the available volume ratios for heat powder are much closer to each other. It is likely that making these changes would not lead to a very

appreciable difference. It is also likely that changes in the heat powder iron/potassium perchlorate ratio would make a larger difference for the available formulations.

While manufacturing and environmental effects are not likely to be significant factors in the resistive activation project testing, awareness of these issues is beneficial to make sure pellets are tested in similar conditions to the largest extent possible. Reinholz and Wesolowski's work (2014) covers the effects of powder age, powder manufacturer, temperature, surface finish, Fe/$KClO_4$ ratio, and deposition of TNT thin film on heat pellet ignition. Consistency of ignition throughout a battery's lifespan and in different environments is important for thermal battery operation. Additionally, reducing supply chain risk by having the option of utilizing different powder vendors is desirable. The results of this paper could give indications of how these factors may affect resistive activation ignition. The age range of the pellets compared spanned four decades. Humidity was kept very low as all the pellets were stored in a dry room. Similarly to other pellet ignition studies, a laser was used to provide the ignition energy for testing, with the ability to control temperature. Testing followed a modified Bruceton method, where increasing length pulses of energy were delivered until the pellet ignited, starting at 200ms and increasing by 25ms each subsequent attempt. Pellets at the lowest temperature tested, -55°C, tended to require significantly more energy than the pellets tested at 25 and 75°C, where there was only a slight difference. This shows that heat conduction may be a large factor in determining how readily a pellet fires. The results of the aging testing were inconclusive but seemed to suggest that age correlated with increased ignition energy. Pellets from different manufacturers showed large differences in ignition energy, but the reasons for this are unknown. There were no observed differences between the different Fe/$KClO_4$ weight ratios used. However, the ratios used for these pellets (86/14

and 88/12) are quite close to each other, and the pellets used had a seven-year age gap. For the resistive activation project, the manufacturing variability concerns will not be a problem if the testing procedures used previously are followed. Pellets are manufactured and stored in a dry room, and testing is conducted at a normal room temperature. Experiments are performed on pellets that are manufactured in a span of one or two months at the most, so aging effects will not cause any differences. The Reinholz and Wesolowski study confirms that pellet manufacturing is an important factor. However, the resistive activation pellets are pressed from powder from one manufacturer and pressed by experienced operators.

A paper by Béquin and Tournat (2010) explored aspects of contact resistance between metallic beads. Contact resistance between iron particles is one factor that determines the resistance of a heat pellet (See Figure 11). To further understand the physics of contact resistance, the authors designed an experiment comprised of stainless-steel beads in contact with each other, with stainless-steel electrodes of the same size as the beads. The beads were arranged linearly and were held together with a weak amount of force. Regulated current was provided by a computer-controlled power supply. Current was increased or decreased over the duration of the test in two-second intervals, and the voltage and current was recorded. When a small current was first applied, the voltage was high, indicating a high resistance. As more current was applied, resistance decreased. As current was decreased from the maximum value, the resistance decreased significantly. Raising current again showed slightly lower resistance. This shows that there is an irreversible change in resistance as the material heats up, caused by the change of contact area between the beads. The diameter of the circular contact area depended linearly on the current. The change in resistance seen in this experiment is mirrored in the TBRA experiments. In a current/voltage plot from a heat pellet

ignition test (Figure 12), the resistance decrease can be seen in the increase in current (red curve) and decrease in voltage (blue) before ignition. Increasing changes in contact area would explain this phenomenon, as well as rising temperature causing the potassium perchlorate to become more conductive.

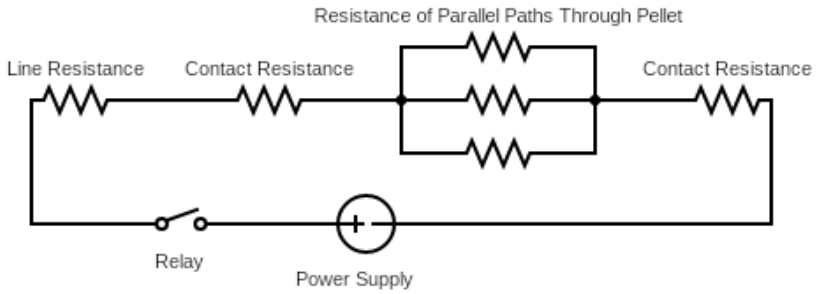

Figure 11. Contributions to circuit resistance

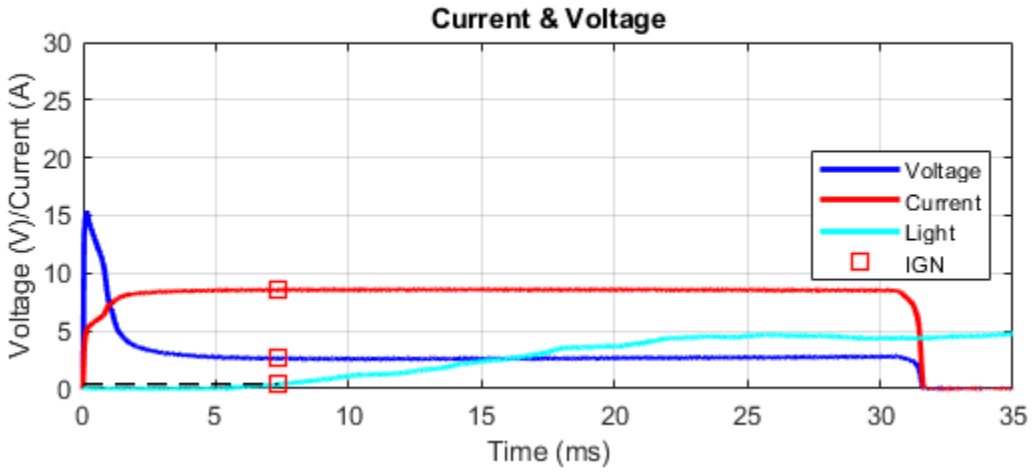

Figure 12. Example of current, voltage, and light vs time plot from heat pellet ignition testing

Because of the pressures present in a thermal battery stack, the electrical behavior of powder under compression is an important phenomenon to understand. This article (Leheup & Moon,

1978) explores the mechanisms behind changes in conductivity due to compression in iron sintering powder. The experimentally measured conductivities from this study were significantly lower than what theoretical models predicted. A thin iron oxide layer can form on the surface of particles, which lowers conductivity. Under compression, the iron particles can deform and expose un-rusted surfaces, and the oxide layer might crack. These phenomena would cause the conductivity to increase, which explains the difference between the theoretical model and real measurements. Data from the testing also showed that reformation of the oxide layer takes place when the applied pressure is released, and that stress cycling caused a continuous loss of conductivity. The pressing force used on the iron particles in this article was up to 240 MN/m^3, compared to pressing forces of between 0.3787 $Tons/cm^2$ (33.69 MN/m^2) and 3.37 $Tons/cm^2$ (299.8 MN/m^2) for 86/14 pellets of the lowest and highest densities. In the ignition testing compression fixture, pellets experience either 100 or 400 psi (0.690 or 2.76 MN/m^2). The pressing force during manufacturing is probably enough to break the oxide layer between particles, but this oxide layer will likely reform as the pellet relaxes. However, the application of force in the compression fixture is likely not high enough to cause a significant change in conductivity between iron particles.

An article by McCarthy et al. (1985) analyzes the burn rate of heat pellets, which is important for battery performance. Testing that assesses burn rate will also indirectly reveal some information about ignitability, as is the case in the experiments described in this article. Heat pellets were pressed to different densities, then fired in a fixture meant to represent the boundary conditions inside a thermal battery. 88/12 and 86/14 powder formulations were used in the test. Five holes in the fixture allowed fiber optic cables to transmit the light emitted by combustion to photodiodes, thereby allowing the burn speed to be calculated. The

pellets were ignited by either a capacitor or a propane torch. The recorded burn rates took a concave down shape when graphed versus density and appeared to reach a maximum for both formulations around 3.5 g/cc (around 55.7% TMD for 88/12 stoichiometry, and 57.6% TMD for 86/14). As density increased, burn rates decreased. Above 4.4 g/cc, ignitions often were quenched, and above 5 g/cc no ignitions were able to be started. These ignition trends are likely similar to the trends that would appear from further testing of pellet density in the context of the resistive activation project. While no pellets for the resistive activation project have been pressed to densities as high as 5 g/cc, higher density pellets have been slower to ignite in ignition tests, showing that the trend should be similar. This suggests that the best density for resistive activation may be 3.5 g/cc as this is the readiest to continue an ignition reaction.

The experimental work described in this thesis was intended to determine the direction of future experiments. A full factorial design was considered, but the number of tests would be much too large and would have cost a considerable amount of time and money. Therefore, a screening design was selected, with the objective of determining the factors that have the largest impact on ignition. While this design does not provide much information about which factor level is optimal, the results give direction for optimizing future experiments. The next section describes the experimental setup, sample preparation, and design of experiments. Then, the subsequent chapters will describe the results of the experiments and data analysis. The conclusions of this work will be used to make a recommendation for further testing and to further understand the mechanics of resistive activation.

Chapter 2. Experimental Setup

2.1 Experiment Overview

To optimize a heat pellet and electrode design that can replace thermal battery igniters and heat paper, determinations need to be made regarding heat pellet pressing density, formulation, particle size, and electrode configuration. The power requirements for ignition should also be well understood, as well as the effect of thermal battery closing force. The experiments described in this thesis do not provide comprehensive examination of these parameters, but rather provide direction for future experimentation.

The factors were chosen to explore the trade space available for heat pellet pressing, electrode design, and power requirements. Additionally, information from previous testing and literature informed which factors were selected. From previous TBRA testing (Padilla 2020) and the literature regarding heat pellet ignition and burn rate testing (Rittenhouse, 1970; Guidotti et al., 2006; Evans, 1984; McCarthy et al., 1985), density was one of the most important factors. The density levels in the experiment reflect the values attainable by manufacturing and in previous testing. Particle size appeared to be a significant variable from previous testing and from the literature. The various mixtures were available and covered small and large sizes for each material. Similarly, iron content was an important variable from past testing and the literature. The iron content levels in the experiment cover the range of Fe/KClO4 ratios that are ignitable and practical for use in thermal batteries. In the previous resistive activation work (Padilla 2020), 0.04”, 0.08”, and 0.12” gap sizes were used, and the effects of the differences between these spacings were small. It should be kept in mind that the electrode design was significantly different. The smaller spacings used in this experiment cover the lower end of the spectrum of possible spacing, and even though the

electrode design is different, the increased knowledge about gap size should be relevant to both designs. The voltage and line resistance levels are chosen to give information about the power requirements for ignition, and even though these are not usually in the control of a battery designer, it is important to understand their effect on ignition sensitivity. The lower bound of 16V/10A and upper bound of 4Ω line resistance are set as representative of the signal applied to thermal battery igniters. The lower bound of line resistance is simply the line resistance of the ignition test circuit. The range of pressures corresponds to pressures present in real thermal batteries.

This large trade space presents a difficulty. Because of time and budget constraints, a limited amount of testing was available. Also, new flexible printed circuit electrode designs were in development at the time of writing. However, conclusions from testing embedded electrodes are likely to be valid for these new generation electrodes. For these reasons, the statistical and experimental analysis tool JMP was used to form a screening experimental design. This choice arose from the many experimental factors and the desire to efficiently use the testing capability. The following table summarizes the factors involved and levels of each factor used in the screening design.

Table 2. Experimental Design

Factor	**Total Levels**	**Values**			
Pellet Density (%TMD (Theoretical Maximum Density))	4	40	50	60	70
Particle Size Mixture	4	Lg/Lg	Lg/Sm	Sm/Lg	Sm/Sm
Fe Content (Weight %)	4	82	84	86	88
Gap Size (in)	3	10	20	40	
Voltage (V)	4	16	20	30	36
Line Resistance (Ohms)	3	0.9	2.5	4	
Pressure (psi)	2	100		400	

As stated before, a full factorial design with all these factors would result in a very high number of tests. While this would be able to narrow down the optimal parameters for ignition, it is not practical. The main effects screening design that was chosen had only 40

runs. This is not designed to provide information about the optimal parameters, but instead, it determines the significance of each factor relative to others. In other words, it describes the direction that future experiments should take.

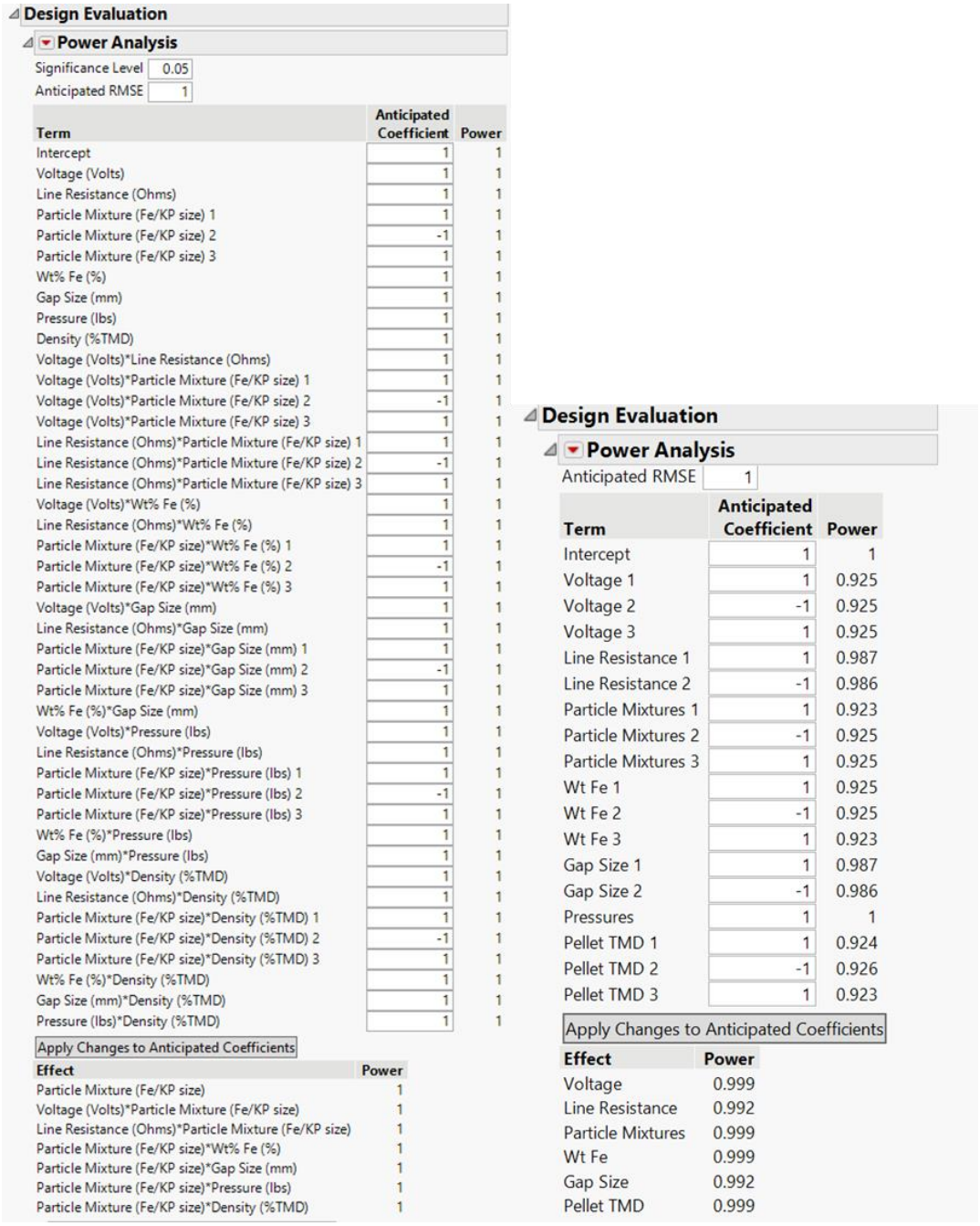

Design Evaluation

Power Analysis

Significance Level 0.05

Anticipated RMSE 1

Term	Anticipated Coefficient	Power
Intercept	1	1
Voltage (Volts)	1	1
Line Resistance (Ohms)	1	1
Particle Mixture (Fe/KP size) 1	1	1
Particle Mixture (Fe/KP size) 2	-1	1
Particle Mixture (Fe/KP size) 3	1	1
Wt% Fe (%)	1	1
Gap Size (mm)	1	1
Pressure (lbs)	1	1
Density (%TMD)	1	1
Voltage (Volts)*Line Resistance (Ohms)	1	1
Voltage (Volts)*Particle Mixture (Fe/KP size) 1	1	1
Voltage (Volts)*Particle Mixture (Fe/KP size) 2	-1	1
Voltage (Volts)*Particle Mixture (Fe/KP size) 3	1	1
Line Resistance (Ohms)*Particle Mixture (Fe/KP size) 1	1	1
Line Resistance (Ohms)*Particle Mixture (Fe/KP size) 2	-1	1
Line Resistance (Ohms)*Particle Mixture (Fe/KP size) 3	1	1
Voltage (Volts)*Wt% Fe (%)	1	1
Line Resistance (Ohms)*Wt% Fe (%)	1	1
Particle Mixture (Fe/KP size)*Wt% Fe (%) 1	1	1
Particle Mixture (Fe/KP size)*Wt% Fe (%) 2	-1	1
Particle Mixture (Fe/KP size)*Wt% Fe (%) 3	1	1
Voltage (Volts)*Gap Size (mm)	1	1
Line Resistance (Ohms)*Gap Size (mm)	1	1
Particle Mixture (Fe/KP size)*Gap Size (mm) 1	1	1
Particle Mixture (Fe/KP size)*Gap Size (mm) 2	-1	1
Particle Mixture (Fe/KP size)*Gap Size (mm) 3	1	1
Wt% Fe (%)*Gap Size (mm)	1	1
Voltage (Volts)*Pressure (lbs)	1	1
Line Resistance (Ohms)*Pressure (lbs)	1	1
Particle Mixture (Fe/KP size)*Pressure (lbs) 1	1	1
Particle Mixture (Fe/KP size)*Pressure (lbs) 2	-1	1
Particle Mixture (Fe/KP size)*Pressure (lbs) 3	1	1
Wt% Fe (%)*Pressure (lbs)	1	1
Gap Size (mm)*Pressure (lbs)	1	1
Voltage (Volts)*Density (%TMD)	1	1
Line Resistance (Ohms)*Density (%TMD)	1	1
Particle Mixture (Fe/KP size)*Density (%TMD) 1	1	1
Particle Mixture (Fe/KP size)*Density (%TMD) 2	-1	1
Particle Mixture (Fe/KP size)*Density (%TMD) 3	1	1
Wt% Fe (%)*Density (%TMD)	1	1
Gap Size (mm)*Density (%TMD)	1	1
Pressure (lbs)*Density (%TMD)	1	1

Apply Changes to Anticipated Coefficients

Effect	Power
Particle Mixture (Fe/KP size)	1
Voltage (Volts)*Particle Mixture (Fe/KP size)	1
Line Resistance (Ohms)*Particle Mixture (Fe/KP size)	1
Particle Mixture (Fe/KP size)*Wt% Fe (%)	1
Particle Mixture (Fe/KP size)*Gap Size (mm)	1
Particle Mixture (Fe/KP size)*Pressure (lbs)	1
Particle Mixture (Fe/KP size)*Density (%TMD)	1

Design Evaluation

Power Analysis

Anticipated RMSE 1

Term	Anticipated Coefficient	Power
Intercept	1	1
Voltage 1	1	0.925
Voltage 2	-1	0.925
Voltage 3	1	0.925
Line Resistance 1	1	0.987
Line Resistance 2	-1	0.986
Particle Mixtures 1	1	0.923
Particle Mixtures 2	-1	0.925
Particle Mixtures 3	1	0.925
Wt Fe 1	1	0.925
Wt Fe 2	-1	0.925
Wt Fe 3	1	0.923
Gap Size 1	1	0.987
Gap Size 2	-1	0.986
Pressures	1	1
Pellet TMD 1	1	0.924
Pellet TMD 2	-1	0.926
Pellet TMD 3	1	0.923

Apply Changes to Anticipated Coefficients

Effect	Power
Voltage	0.999
Line Resistance	0.992
Particle Mixtures	0.999
Wt Fe	0.999
Gap Size	0.992
Pellet TMD	0.999

Figure 13. Comparison between power of full factorial design (left) and main effect screening design (right)

In this type of design, the power of a factor is the probability of detecting a factor's effects, if the effects exist. Power is measured on a 0-1 scale, with 1 being the most desirable. For this design using 40 tests, each factor had a power of at least 0.923, which is well within the acceptable range. Additionally, no confounding effects were predicted.

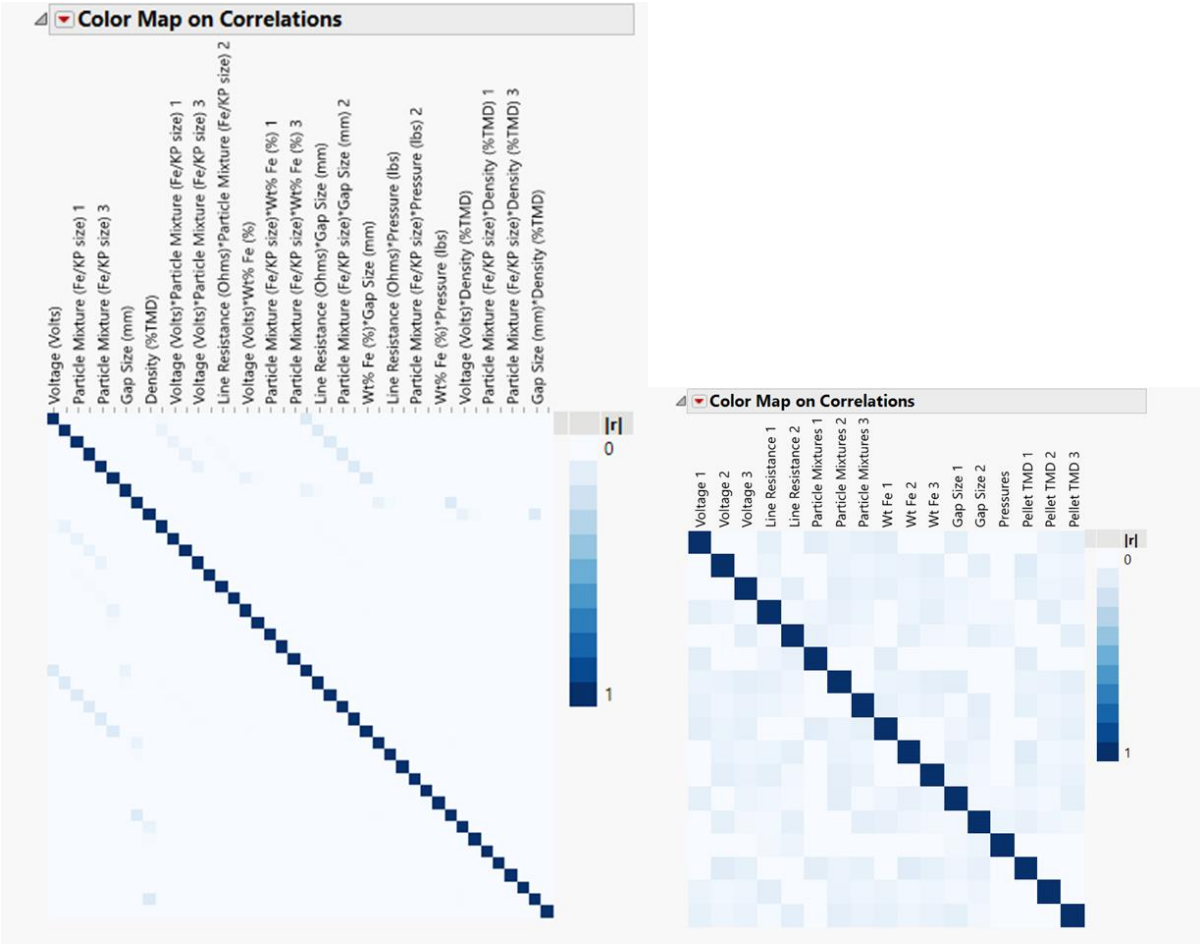

Figure 14. Correlation color map for full factorial design (left) and main effect screening design (right)

2.2 Sample Preparation

The samples used in the tests are heat pellets with twisted wire electrodes embedded in them (Figure 6). They were manufactured at Sandia National Labs by skilled technologists. The processes described here are intended to repeatably produce repeatable high quality heat pellets.

2.2.1 Electrode Manufacturing

The first step of sample preparation is to manufacture the wire electrodes. These are made of twisted Kapton wire with a loop at the end, cut to provide a gap. The equipment needed for this process is as follows:

1. Kapton insulated silver coated copper 34 gauge wire, from Accuglass
2. Flexible 5/8” diameter grommet
3. Bench vise
4. 0.100” diameter dowel (or #00 Philips screw driver)
5. Dremel mandrel for holding cutting disks with screw.
6. Power drill
7. Precision cutting knife
8. Small flat screwdriver
9. Ruler, 12 inch or longer
10. Tweezers
11. Heavy duty scour pad (Scotch-Brite™)

To manufacture the electrodes, the first step is to cut a 12-inch length of 34 gauge Kapton-insulated silver coated copper wire. Since the wire is very thin, it should be handled with care throughout all steps of the sample preparation process. After it is cut, the wire should be bent halfway through so that the cut ends are matched in length. The cut ends should be formed into a loop and screwed into the mandrel.

Figure 15. Wire and mandrel

The mandrel should be placed and secured into a drill chuck. Next, a 0.1-inch dowel rod or #00 Philips screwdriver shaft is clamped into a vise so the dowel rod or shaft is vertical. The looped end of the wire is placed around the rod and pulled taut. The vinyl grommet is inserted between the wires about an inch from the drill chuck.

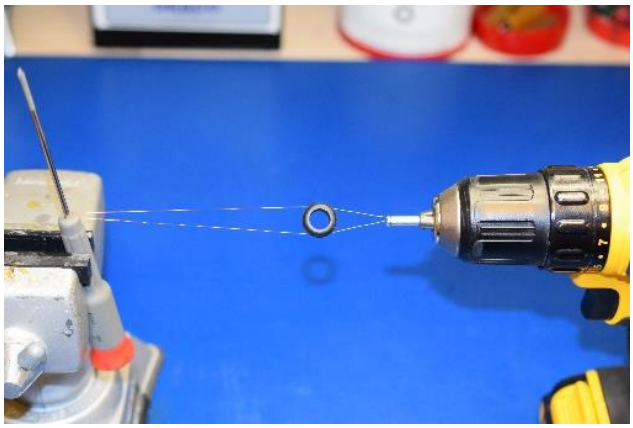

Figure 16. Setup for twisting wires

While the grommet is held by hand, the drill should be turned on at the slowest speed to twist the wires between the mandrel and grommet. Once this is complete, the grommet is released to twist the wires between the grommet and dowel rod. The drill is spun until the wires break near the mandrel. The wire should be supported and removed from the dowel, then the wires are cut on the mandrel side of the grommet. The Kapton at the leads should be removed with

a knife and/or a scour pad, resulting in a bright and shiny surface. Then, the loop is cut with a knife to the desired gap size.

The Kapton on the wire loop end is removed using a Coherent brand manual laser welder. The proper settings were determined by experimenting with the welder's energy and spot size controls and viewing the resulting wire under a microscope. The settings that resulted in full Kapton ablation without melting the copper are as follows:

Table 3. Laser Welder Settings

Parameter	**Value**
Power	0.15kW
Laser Duration	2.7ms
Spot Size	0.4mm

Each wire tip was hit with the laser beams once on each side of the loop, with four hits in total to fully ablate the Kapton from the wire tips. After this is complete, the wires are examined using an optical microscope to verify that the Kapton has been removed. As seen in Figure 17, the rightmost wire has bare copper exposed without melting.

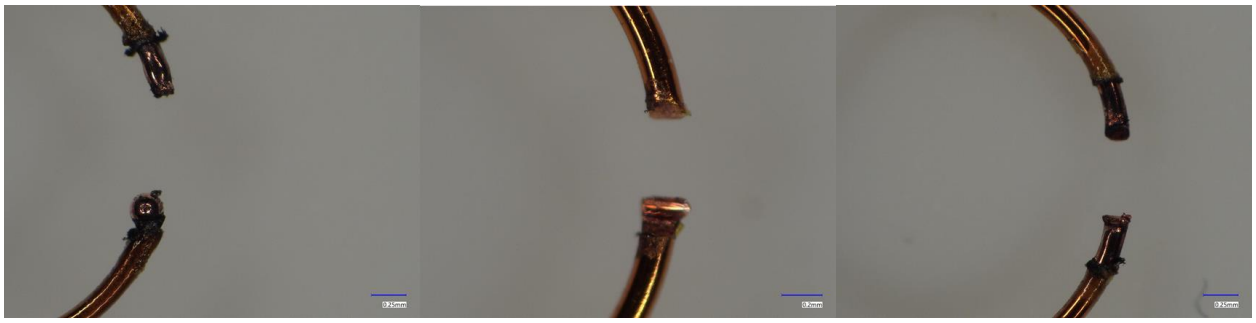

Figure 17. Comparison between three different laser welder settings. Left: 3ms – 0.15kW, Middle: 1ms – 0.15kW, Right: 2.7ms – 0.15kW.

Even with the optimal 0.15kW/2.7ms energy settings, microscope pictures of the wires revealed that there was a fair amount of variability between electrode contact areas. This

variability is likely due to the ablation process being done by hand. These electrodes were used for testing, but the differences in contact area between electrodes may explain some of the variability in measured pellet resistance and ignition performance.

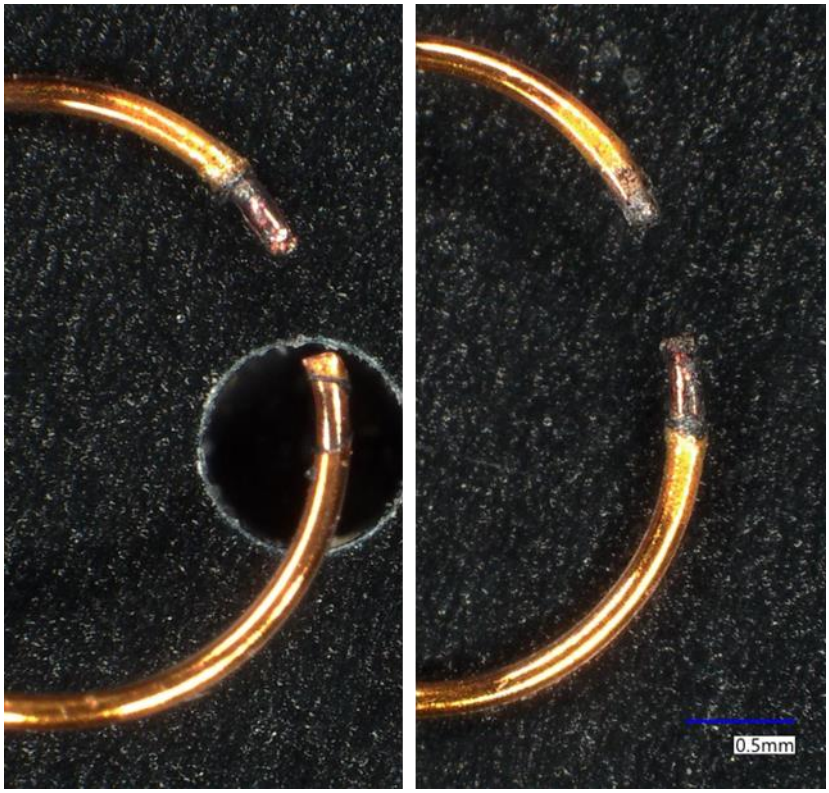

Figure 18. Comparison between two electrodes made subsequently, showing visual differences in Kapton ablation

2.2.2 Powder mixing and particle sizing

Before mixing the potassium perchlorate and iron powder together, part of each powder batch needs to be processed to reduce particle sizes. To do this, the potassium perchlorate powder is ball milled and the iron powder is sieved.

The equipment required for ball milling includes a U.S. Stoneware ball miller used with a 1-liter plastic milling vessel inside of a heavy roller sleeve. The media used are 10mm spherical

Yttria-doped Zirconia beads. Other equipment required include #40 and #60 sieves, and a vacuum oven.

The milling vessel is filled halfway with milling media, and 75-80g potassium perchlorate is added. The vessel's lid is secured with tape around the seal joint and put into the milling sleeve, so that the vessel is centered within the sleeve. The vessel and sleeve are placed onto the ball mill rollers, and a speed of <= 50% is selected. The mill is operated from 8-16 hours. After ball milling has concluded, a #40 US Mesh sieve with collection pan is used to separate the mixing media and the powder. The powder is sieved once more through a #60 US Mesh sieve and vacuum dried at 115 C for 16 hours at 25" Hg vacuum.

To obtain the desired iron powder particle sizes, a sieving process is used. The equipment used includes assorted US Mesh sieves, a ROTAP™ 8" sieve shaker (model RX-29, SN 10-5405), a powder scoop, and a digital scale. The sieves are placed in a stack five high with the larger meshes at the top and a collection pan at the bottom. The timer on the sieve shaker is set for 15 minutes.

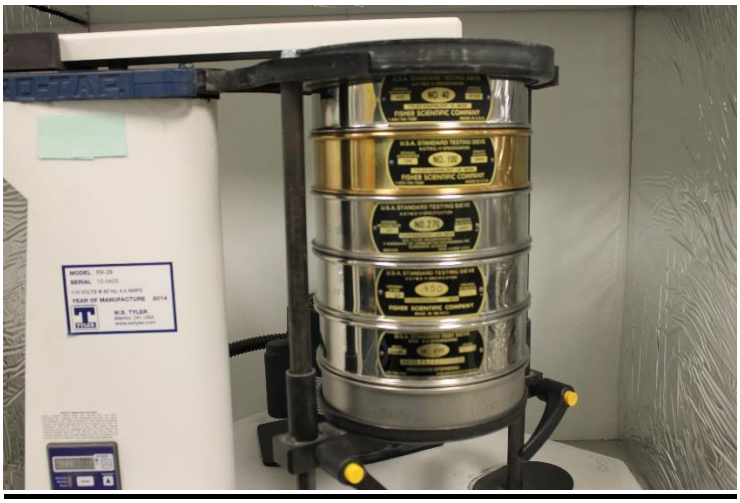

Figure 19. Sieve stack

2.2.3 Heat Pellet Pressing

The embedded electrode pellet pressing procedure is similar to the procedure for pressing normal pellets. The equipment used for pressing consists of a Wabash hydraulic press, a pellet press die with machined slots, 3D printed die slot inserts, stripping fixture, and a powder leveling tool. Once powder has been mixed and weighed, pressing can begin.

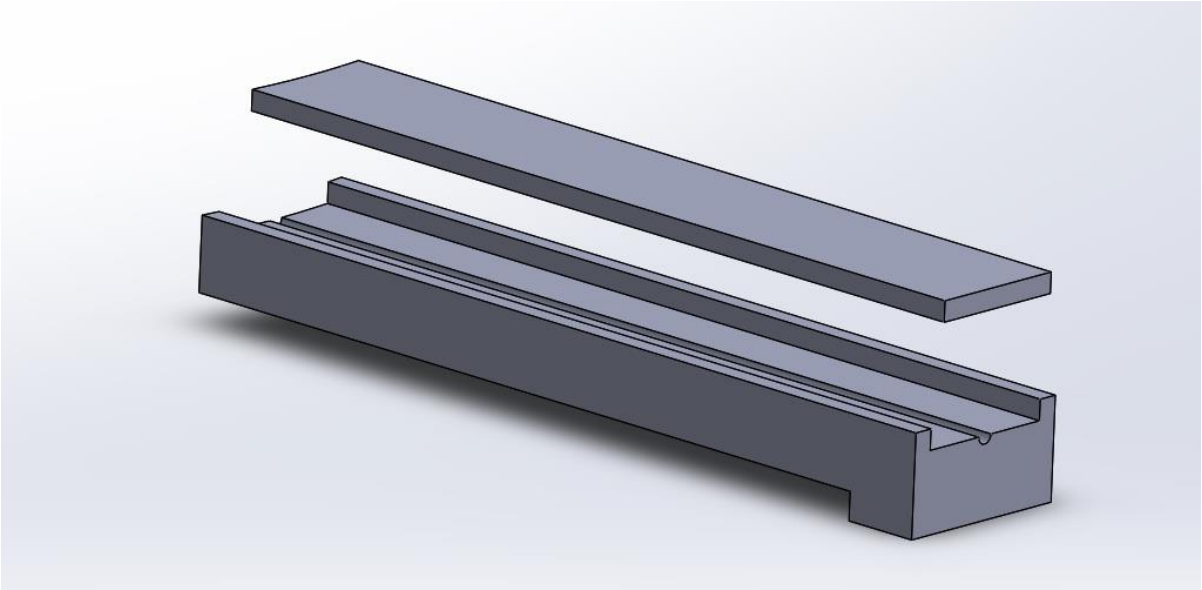

Figure 20. Model of die slot insert

Before beginning pellet pressing, the pocket depth will be set for the amount of powder to be pressed. Once this has been done, the pellets to be used in the experiment can be pressed. The first step is to secure the wires in the inserts. The die inserts are 3D-printed parts that sit in the machined slots in the pellet pressing die. The inserts have channels for the wires to sit and a lid that holds the wires in place.

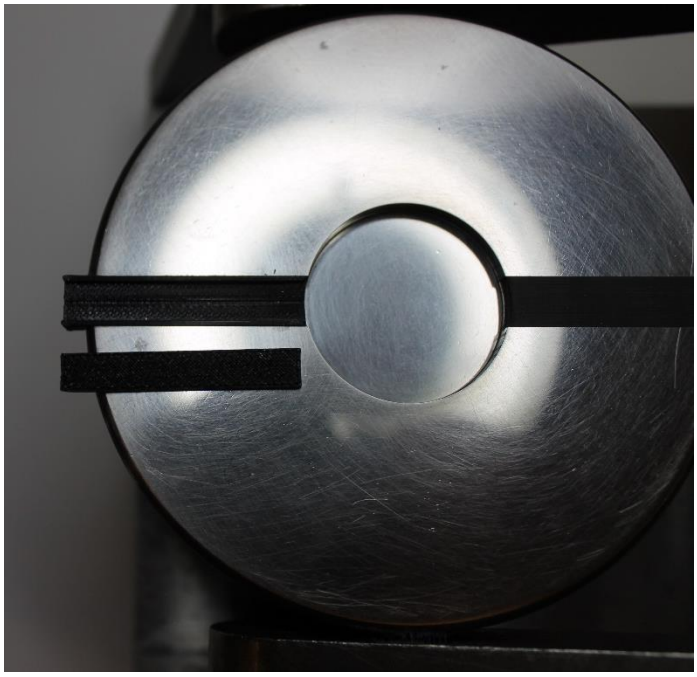

Figure 21. Pellet press die machined to accommodate 3d printed inserts (installed)

The wire should be placed in the insert such that the tips are located in the center of the die, with the curved end of the insert facing the inside of the die. The loop of the wire should be positioned horizontally in parallel with the surface of the die. The cap should be pressed in once the wire is in place such that the curved side is facing the inside of the die. Once the insert is in place, the wire should be pushed down lightly to give it a slight downward angle. This helps the wire stay inside the pellet during pressing.

Figure 22. Wabash hydraulic press

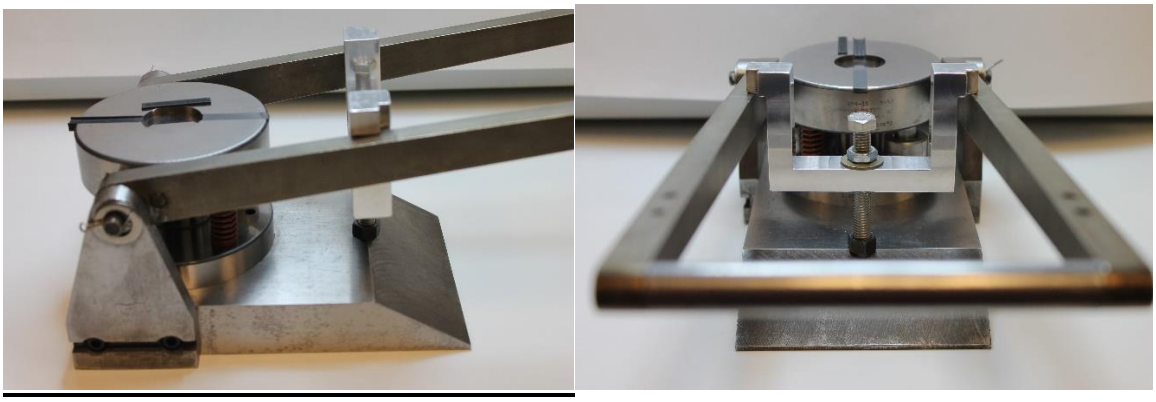

Figure 23. Stripping fixture, pellet die, and stripping arm stay setup

The stripping fixture, pellet die, and stripping arm stay assembly should be slid into the press slightly. The powder then is added into the pocket and smoothed using a leveling blade or scraper. The assembly is then slid fully into the pressing position against the back plate. The lower crossbar is mounted to secure the assembly in the baseplate. The press is engaged, and when it switches to stripping force, the stripping arm handle should be pulled gently down to strip the pellet. The wire may lift the cap off the insert. After stripping the pellet and

releasing the press, the cap should be removed with tweezers and set aside to allow for the removal of the pellet from the die. The pellet will shed some powder around the edges due to height variations between the die and the inserts. The excess powder should be gently removed from the pellet surface and edges. A pencil is used to mark the location of the wire end or wire loop to aid in positioning the fiber optic cable during testing. All the excess powder in the die should be cleaned and disposed of. The die and inserts should be wiped with a cloth lightly wetted with methanol. The pellets then should be vacuum dried overnight at 100° C. After this, they are packaged for storage in vacuum sealed plastic envelopes.

2.3 Test Setup

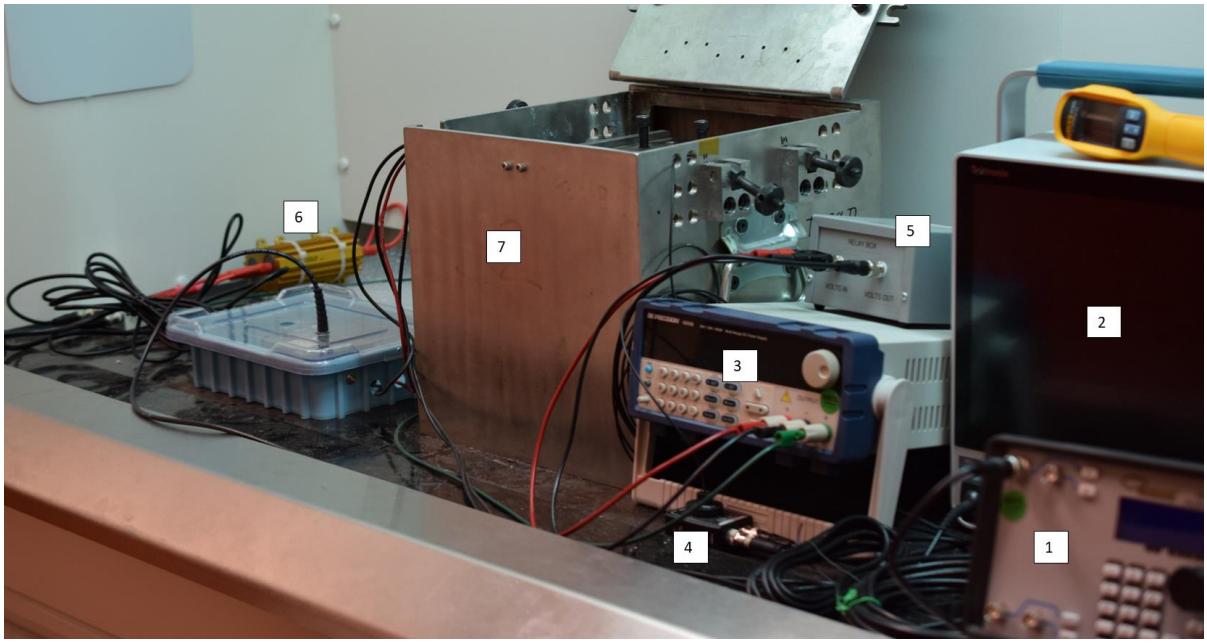

Figure 24. Ignition tester setup

Equipment list:

1. Pulse Generator: Quantum Composers 9520 Series w/ 2 Output Channels
2. Oscilloscope: Tektronix MS058 8-Channel Digital

3. Power Supply: BK Precision 9205B (DC, 60W, 25A, 600W)
4. Light Detector: Thor Labs DET10A2 with Thor Labs Power Supply
5. Relay: Potter and Brumfield SSRDC-200D25
6. Resistor Pack
7. Boombox: Custom Made at SNL. ¼" thick Aluminum Box with Latched Lid
8. Load Cell: Omega Engineering Digital Load Cell (In Back of Test Fixture)
9. Test Fixture: Custom Designed at SNL
10. Resistance Tester: Valhalla Scientific 4314A Digital Igniter Tester
11. Current Viewing Resistor: KTECH Corp CVR.1 – In Plastic Box

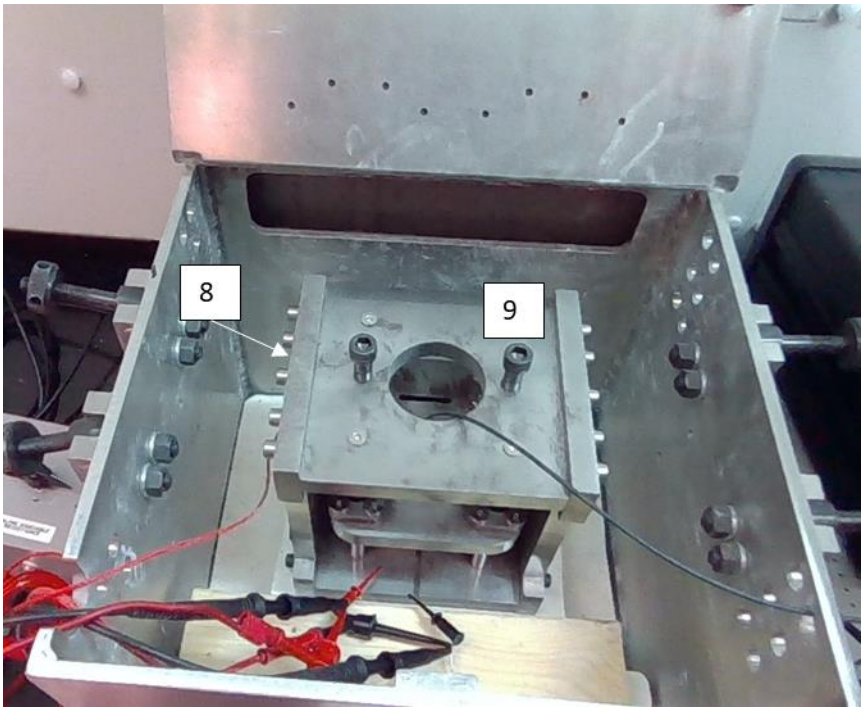

Figure 25. Boombox and test fixture

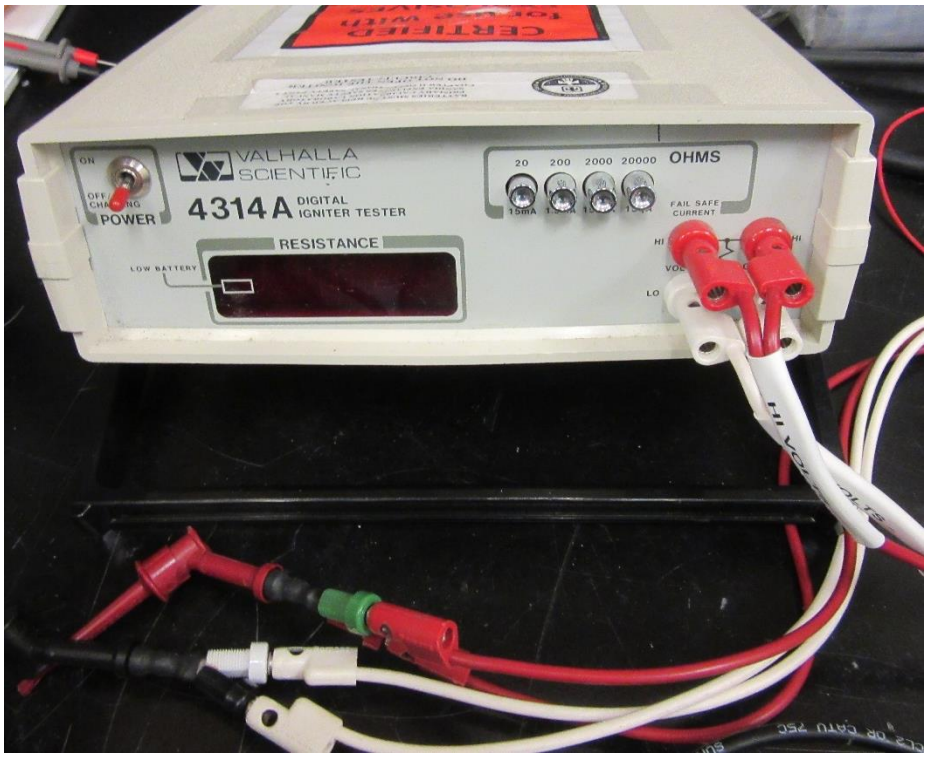

Figure 26. Valhalla 4314A Digital Igniter Tester (10)

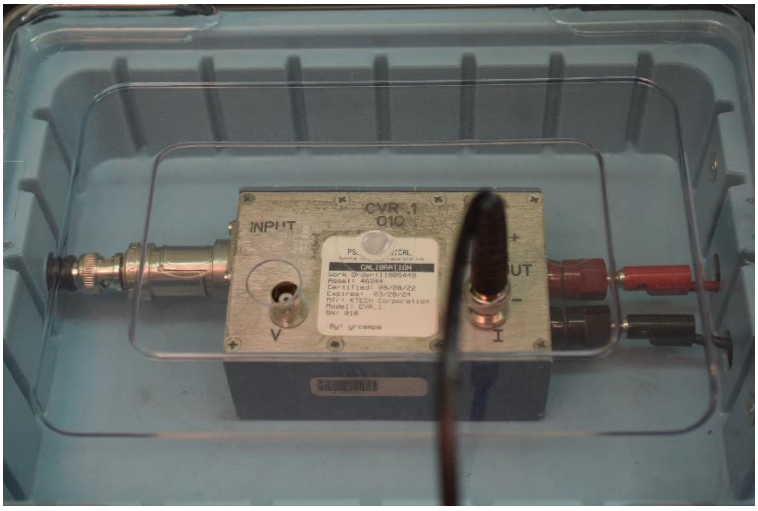

Figure 27. CVR (current viewing resistor) (11)

The experimental setup for ignition experiments is intended to deliver a pulse of current at constant voltage to a heat pellet. The data recorded includes voltage across the pellet, the current through it, and amount of time before ignition. To determine the time of ignition, a fiber optic cable positioned close to the electrodes carries light to a light level detector, which

sends a corresponding voltage signal to an oscilloscope. A current-viewing resistor is used to determine the amount of current flowing through the circuit, and voltage probes are used to determine the voltage drop across the pellet. Both current and voltage are recorded on the oscilloscope, which is set to trigger when probe on the high side of the heat pellet reaches 2.2 volts.

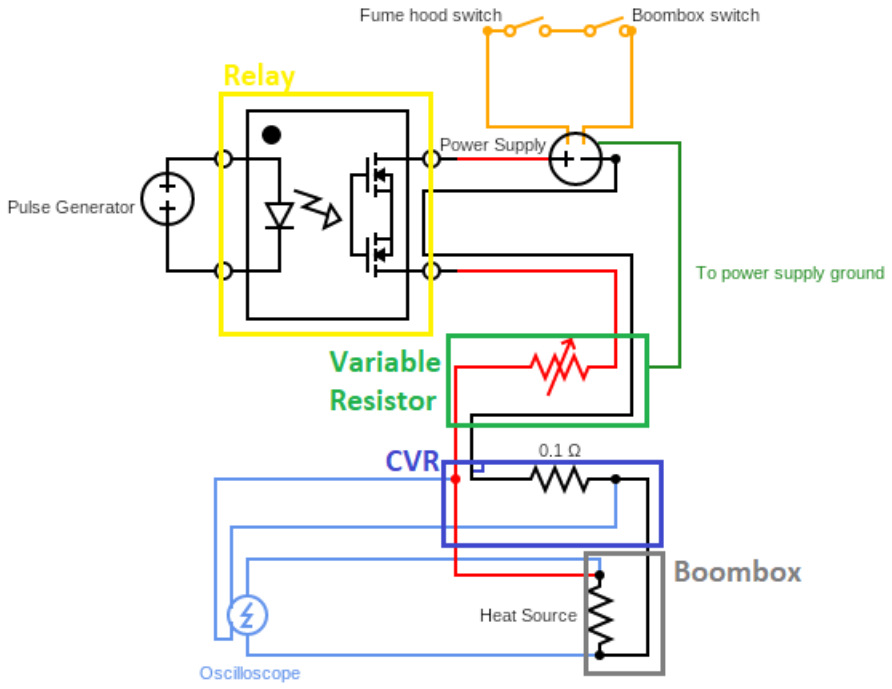

Figure 28. Ignition circuit diagram

As seen in the circuit diagram above, a power supply is connected to the ignition circuit through a relay, which is closed and opened by a pulse generator set to output a 30ms pulse. The relay is needed so that the window of time the circuit is closed is well controlled and repeatable. The rise time of a power supply is too long to represent the conditions of the system the heat pellets are designed for, but the relay is able to provide a very fast rise time. Also, the relay provides some safety in the event the power supply is enabled while a test

operator has exposure to points in the circuit that may become shock hazards, as well as preventing accidental ignitions.

The circuit is almost entirely contained within a fume hood to provide physical separation from shock hazards, burn hazards, and powder and smoke from heat pellet ignitions. The test is initiated from outside of the fume hood by the pulse generator. Within the fume hood, the compression fixture sits inside a metal boombox to further contain ignition products.

During initial testing of the setup and before the experiments described in this work, a problem was revealed with the initial version of the test setup which needed to be solved before further testing took place. A banana jack to BNC adapter connected the outputs of the power supply to a BNC cable running to the relay box. When line resistance measurements were taken, this connector was unplugged from the power supply to attach the resistance tester leads to the circuit. However, since the connector was unmarked and could be flipped upside down, the potential for reversing the circuit polarity was present. During a pellet ignition test the connector was inserted upside down, reversing the polarity of the circuit and bypassing the open relay. When the power supply was enabled, a heat pellet activated unexpectedly before the pulse generator triggered the closing of the relay. While there was no shock, burn, or injury associated with the incident, it prompted further consideration about the design and the safety of the setup. Additionally, even though the oscilloscope triggered from the ignition, no useful data was collected since the ignition signal was not gated by the relay. This allowed a pulse of power longer than the standard 30ms to reach the pellet.

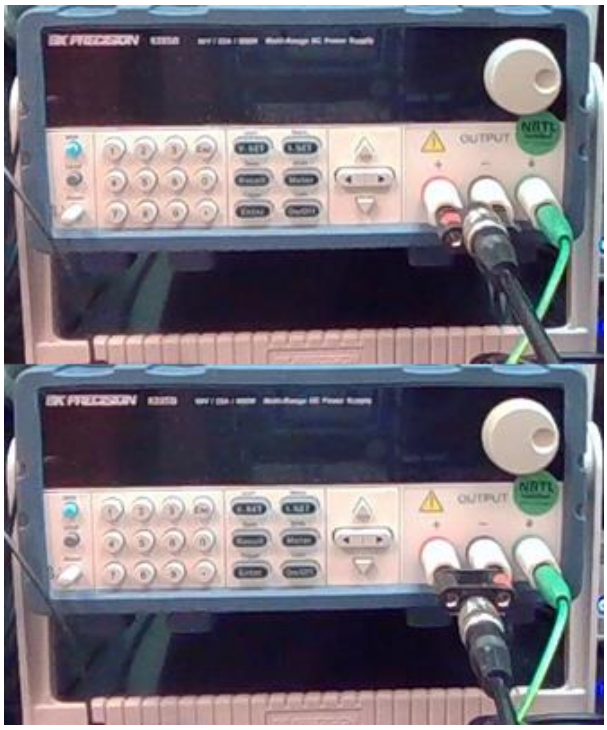

Figure 29. Difference between normal and flipped connector. The red dot on the positive side was added after the incident

With these concerns in mind, the following changes were made to increase safety and reliability of the ignition setup:

- The banana jack to BNC adapter was changed. Instead of a black adapter connected directly to the power supply, color-coded (red and black) leads from the power supply outputs were connected to a color-coded banana jack BNC adapter. This made visual checks of the polarity of the circuit much simpler and quicker (Figure 30. Change made to power supply leads and BNC adapter).

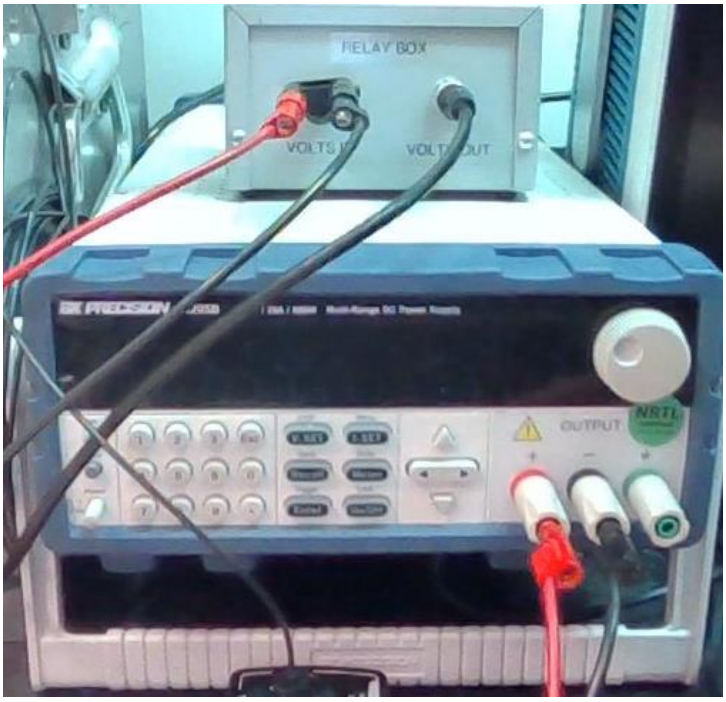

Figure 30. Change made to power supply leads and BNC adapter

- The CVR box was further contained in a plastic container, as it was determined that the box was metal and presented a shock hazard.
- The metal variable resistor box previously had uninsulated external BNC connectors leading to the internal components. These were replaced with insulated connectors to prevent the box from becoming a shock hazard. The variable resistor ended up being replaced with a fixed resistor with insulated connections for the final iteration of the test setup.
- The pulse generator was moved outside of the boombox to further isolate workers from hazards.
- The testing procedure was evaluated and revised to include checks and safeguards for safe operation. While the leads are being connected to the unit under test, or while an operator's hands are inside the boombox, the leads are to be disconnected from the

CVR and shorted together. A visual and verbal check was also instituted to confirm that operators had no contact with the circuit.

Before testing is started for the day, a “ringdown” test is run, which involves the same process as a pellet test, but using a 1-Ohm dummy load resistance instead of the heat pellet. Since this resistance is known and does not change, the waveforms recorded on the oscilloscope can be checked to make sure all the equipment is set up correctly.

Step by step, the testing procedure is as follows:

1. Before testing heat pellets, perform a ringdown test:
    a. Plug in all equipment
    b. Turn on oscilloscope, light detector, and pulse generator. Not power supply
    c. Take a line resistance measurement
    d. Disconnect leads from CVR
    e. Short leads at the CVR
    f. Check relay function with handheld multimeter
    g. Connect ignition circuit leads to dummy load
    h. Connect leads to CVR
    i. Turn on power supply
    j. Check pulse generator and power supply settings
    k. Set oscilloscope
    l. Lower hood to ¾, and make sure (Visual/Verbal check) that hands are not near areas that could be live (CVR, BNC sheaths).
    m. Enable power supply output
    n. Lower hood all the way

o. Activate pulse generator

p. Open the hood

q. Disable power supply output

r. Save Oscilloscope results with naming convention found in test matrix

2. Heat Pellet Testing

a. Turn off power supply

b. Take resistance measurement of pellet using explosive-safe resistance tester

c. Insert pellet in between mica sheets

d. Insert pellet/mica into test fixture, aligning mark with slot in fixture

e. Move fixture inside boombox

f. Align fiber optic cable

g. Compress pellet to target force

h. Record pellet resistance measurement/force measurement

i. Record line and pellet resistance measurement

j. Disconnect leads from CVR

k. Short leads at CVR

l. Connect leads to pellet

m. Connect leads to CVR

n. Turn on power supply, but do not enable

o. Check pulse generator/power supply settings

p. Set oscilloscope

q. Lower hood to ¾, and make sure (Visual/Verbal check) that hands are not near areas that could be live (CVR, BNC sheaths).

r. Activate power supply

s. Lower hood all the way

t. Activate pulse generator

u. De-activate & turn off power supply

v. Save Oscilloscope results on computer with naming convention found in test matrix

w. **If pellet doesn't activate, wait 5 minutes before removing it from fixture**

x. Record pellet resistance/force

y. Unload pellet

z. Record unloaded post-test resistance

aa. For testing more pellets, return to step **b**

Waveform files saved by the oscilloscope are in a comma separated variable format. The oscilloscope collects 40ms of data with a sample rate of 3,125,000 samples per second. A MATLAB program is used to process and plot the data, calculating dynamic resistance, power, and cumulative energy from the voltage and current data. The program is able to determine the time of ignition from the light out data, which aids in understanding ignition conditions by obtaining voltage and current values at that time. The program also generates plots showing voltage, current, dynamic resistance, power, and cumulative energy versus time.

Before the test, the pellet resistance is measured prior to compression, then again under the full compressive load in the ignition fixture. Line resistance is measured before the test while under compression, as well as the total circuit resistance including the pellet. Within a minute

after the test, the total circuit resistance including the pellet is measured, and then the pellet is measured once it has been removed from the test fixture and circuit.

Chapter 3. Data

Forty ignition tests were performed with twenty-eight pellets reaching ignition (referred henceforth as “go” tests.) Several of the low-density pellets cracked before testing while the pellets were being handled. One pellet cracked through the middle, and since the resistance readings were over the 20kOhms limit of the resistance tester, the pellet was remade.

Table 4. Experimental Data

TN	11	31	41	3	82
SN	1	2	3	40	Go
Fe wt%	84	88	82	40	Go
Particle Size Mixture	SV-BM	SV-AR	AR-AR	AR-AR	SV-BM
Target % TMD	70	40	40	40	50
Real Density (g/cc)	4.096635	2.544704	2.538406	2.538406	3.136696
Real %TMD	69.63278	40.52386	44.5362	44.5362	49.95121
Gap Size	10	40	40	40	20
Target Pressure (psi)	100	100	100	100	100
Unloaded Pre-Test Pellet R (Ω)	3.968	43.02	35.59	35.59	8.882
Target Force (lbf)	122.7185	122.7185	122.7185	122.7185	122.7185
Pre-Test Measured Force (lbf)	123.8	123.9	123.9	123.9	123.2
Loaded Pre-Test Pellet R (Ω)	4.329	61.74	42.02	42.02	8.602
Loaded Pre-Test Line + Pellet	4.908	58.65	43.21	43.21	12.743
Desired Line R (Ω)	0.9	4	4	4	4
Measured Line R (Ω)	0.614	3.945	3.946	3.946	4.046
Power Supply Voltage (V)	16	20	30	30	36
Result	Go	Go	Go	Go	Go
Function Time (ms)	4.138	17.136	3.131	3.131	5.282
Post-Test Measured Force (lbf)	15.2	19.2	11.7	11.7	24.9
Loaded Post-Test Pellet+Line R (Ω)	1.236	4.302	4.215	4.215	4.27
Unloaded Post-Test Pellet R (Ω)	1.421	0.532	0.502	0.502	0.672
Noisy Data	n	n	y	y	n
Notes		Replace	Redo of	Grabbers	

Table 4. Experimental Data (cont.)

14	36	1	22	13	35	34	21	12	33
14	13	12	11	10	9	8	7	6	5
84	88	82	86	84	88	88	86	84	88
SV-BM	AR-BM	SV-BM	AR-AR	AR-BM	SV-BM	AR-AR	AR-BM	SV-AR	AR-BM
50	60	60	40	40	40	70	60	60	40
3.519688	3.773772	3.423955	2.535909	2.620569	2.626392	4.442156	3.651319	3.534859	2.615663
59.82609	60.09651	59.96607	41.74403	44.54326	41.82474	70.74038	60.10498	60.08396	41.65388
10	20	10	10	10	20	40	20	40	10
400	400	400	100	400	100	400	400	100	400
77.6	1.685	16	19.28	25.02	42.47	4.413	4.989	4.979	755.6
490.8739	490.8739	490.8739	122.7185	490.8739	122.7185	490.8739	490.8739	122.7185	490.8739
492	490.6	488.1	124	494.2	124.4	493.4	493.4	125.1	490.6
172.13	1.715	12.64	22.7	58.82	46.61	4.996	5.527	4.669	202.3
174.94	5.85	12.596	26.52	62.74	46.64	7.105	7.553	5.195	99.43
4	4	0.9	4	2.5	0.9	2.5	2.5	0.9	0.9
3.874	4.033	0.718	3.957	2.43	0.659	2.549	2.633	0.614	0.643
20	16	36	30	20	16	36	30	20	16
Go	No Go	Go	Go	Go	Go	No Go	Go	Go	Go
1.758		2.628	3.612	5.671	6.884		3.795	3.635	2.079
24.3	489.6	16.3	19.5	12	14.2	492.5	70.3	13.6	63.7
4.486	6.715	2.524	4.145	3.206	0.837	3.501	2.62	1.009	0.983
1.133	1.97	2.877	0.261	1.379	5.3	1.091	0.291	0.627	0.455
n	n	n	y	y	n	n	n	n	y
A little		Resistan	Piece of	Pellet	Post test			Replace	Light out

Table 4. Experimental Data (cont.)

19	6	5	18	17	16	4	23	3	15
24	23	22	21	20	19	18	17	16	15
84	82	82	84	84	84	82	86	82	84
SV-AR	SV-BM	AR-AR	AR-AR	AR-AR	SV-BM	SV-AR	SV-BM	AR-BM	AR-BM
40	40	60	50	70	60	50	50	50	50
2.610117	2.866342	3.46674	2.924602	4.069189	2.954953	2.845867	3.06465	2.862316	2.948293
44.3656	50.3224	60.84277	49.71108	69.16626	50.22697	49.97172	50.44772	50.14706	50.11377
20	20	20	20	20	40	20	40	20	10
400	400	100	100	400	400	400	100	100	100
	63.3	9.595	3.974	2.229	4.968	11.707	17.898	35	8.008
490.8739	490.8739	122.7185	122.7185	490.8739	490.8739	490.8739	122.7185	122.7185	122.7185
492.2	492.2	124	124.7	490.7	492.3	491.1	123.2	124.7	125.3
	79.58	3.73	4.816	2.374	5.61	12.173	21.07	22.52	8.145
	81.96	5.997	7.141	2.866	5.974	15.999	23.57	22.98	11.963
2.5	2.5	2.5	2.5	0.9	0.9	4	2.5	0.9	4
2.4	2.387	2.386	2.395	0.578	0.582	3.857	2.44	0.607	3.905
36	30	20	16	36	30	20	16	36	30
Go	Go	No Go	Go	Go	Go	Go	Go	Go	Go
0.316	3.475		12.628	9.951	3.52	7.617	23.475	3.978	7.708
15.7	11.7	123.5	17	29.1	20	27.1	24.8	8.7	18.4
3.065	11.62	3.416	2.685	1.779	1.723	4.34	N/A	7.457	4.376
0.839	18.5		0.389	7.535	3.388	7.85		5.32	0.805
y	y	n	n	n	n	n	n	y	n
twisted							Replace	Pellet	

Table 4. Experimental Data (cont.)

9	28	27	26	38	8	25	37	24	7
34	33	32	31	30	29	28	27	26	25
82	86	86	86	88	82	86	88	86	82
AR-BM	AR-AR	SV-AR	SV-AR	AR-AR	AR-AR	AR-BM	SV-BM	SV-BM	SV-AR
70	50	60	70	60	60	70	70	70	70
4.037729	3.025975	3.65056	4.259792	3.801168	3.454711	4.272999	4.375278	4.257128	4.031624
70.83711	49.81109	60.09249	70.12116	60.53279	60.49209	70.33857	69.67537	70.0773	70.66177
40	40	10	20	10	10	10	40	20	40
100	400	100	100	100	400	100	100	400	400
8.742	2.566	2.328	2.655	2.159	8.062	2.818	2.325	2.029	4.006
122.7185	490.8739	122.7185	122.7185	122.7185	490.8739	122.7185	122.7185	490.8739	490.8739
124	491.7	122.7	123.5	123.1	492.3	123.4	122.3	491.7	491.5
8.702	2.912	2.372	4.438	1.906	9.035	2.902	2.182	2.202	4.302
9.232	3.321	4.674	4.993	2.521	9.121	6.473	5.277	6.03	8.016
0.9	0.9	2.5	0.9	0.9	4	4	2.5	4	4
0.58	0.57	2.418	0.583	0.689	3.91	3.939	2.461	3.935	3.89
20	16	36	30	20	16	36	30	20	16
No Go	Go	Go	Go	No Go	No Go	No Go	No Go	No Go	No Go
	6.45	3.429	2.285						
122.2	47.7	22.3	19.1	122.2	490.7	122.8	121.8	491	485.5
2.608	1.033	2.798	1.265	1.408	5.999	6.106	3.808	6.059	5.934
1.94	1.377	0.761	3.039	0.869	2.713	2.188	1.434	2.198	2.291
n	n	n	n	n	n	n	n	n	n

Table 4. Experimental Data (cont.)

30	40	29	10	20	39
40	39	38	37	36	35
86	88	86	82	84	88
AR-AR	SV-AR	AR-BM	SV-AR	AR-BM	SV-AR
40	50	50	40	60	70
2.528699	3.130286	3.062058	2.57531	3.538227	4.382316
41.62534	49.84913	50.40506	45.23756	60.14121	69.78744
40	10	40	10	40	10
400	400	400	100	100	400
7.828	6.338	6.271	262.2	3.823	1.431
490.8739	490.8739	490.8739	122.7185	122.7185	490.8739
492.8	493.1	492.5	124.4	124.2	491.4
14.852	7.225	5.786	173.75	3.771	1.492
15.29	8.058	7.906	173.9	7.63	3.746
0.9	0.9	2.5	2.5	4	2.5
0.568	1.105	2.375	2.37	3.918	2.41
36	30	20	16	36	30
Go	Go	Go	Go	No Go	No Go
4.253	2.925	28.326	3.635		
24.6	93.3	41.9	10.1	123.5	490.8
0.787	0.901	2.594	7.727	6.286	3.449
0.278	0.482	0.357		2.508	1.259
y	n	n	n	n	n
Pellet		Replace	Wire fell		

Table 5. Matlab data for ignited pellets

13	35	21	12	33	32	41	31	11	TN
10	9	7	6	5	4	3	2	1	SN
17.36948	3.634495	3.751707	4.982137	13.52956	2.685818	17.14844	8.738405	2.957326	Matlab Voltage at Ign
1.059434	10.68483	10.98363	13.84567	4.267054	8.513475	3.339179	2.821073	10.5458	Matlab Current at Ign
16.39506	0.340155	0.341573	0.359834	3.170702	0.315478	5.135527	3.097546	0.280427	Matlab DR at Ign
18.40181	38.83398	41.20735	68.98105	57.73134	22.86564	57.26171	24.65168	31.18737	Matlab Power at Ign
19.63075	15.76614	9.616725	14.89907	15.67113	15.4162	21.90604	15.4687	9.787189	Matlab Max Voltage
3.162791	14.78225	11.00764	15.35718	5.004057	8.580188	5.460117	2.823554	17.07437	Matlab Max Current
38.93843	113.2437	80.78795	169.9393	64.75471	79.59091	71.54632	25.394	116.677	Matlab Max Power
155.4789	370.8529	238.2388	493.6782	79.88802	192.8867	174.1898	401.4136	257.7434	Matlab Cumulative Energy
26.7021	60.71117	61.37139	131.8923	42.04987	35.63317	52.81807	23.36234	60.82985	Matlab Avg Power

Table 6. MATLAB data for ignited pellets (cont.)

18	17	16	4	23	3	15	14	1	22
21	20	19	18	17	16	15	14	12	11
1.946867	3.133289	5.277208	1.740785	2.562757	20.13059	2.299538	2.266775	4.065742	18.31373
6.003666	10.04836	14.05708	4.718541	5.615792	11.15307	7.127257	4.623519	12.48768	3.020545
0.32428	0.311821	0.375413	0.368924	0.456348	1.804936	0.32264	0.490271	0.32558	6.063056
11.68834	31.48441	74.18215	8.213964	14.39191	224.5179	16.3894	10.48048	50.77167	55.31745
7.128449	18.13256	21.8034	8.183887	12.35963	30.72995	11.32121	14.70732	23.13113	28.49364
6.053452	34.53304	19.34765	4.758537	5.65109	33.01852	7.183104	4.632392	35.43062	5.151497
27.00242	598.6387	380.7851	24.94658	27.43548	581.1515	54.4718	27.77875	598.08	74.91855
244.8997	873.057	743.3985	135.444	592.1979	1179.53	179.4167	38.11761	646.7361	226.7593
19.19036	87.00223	208.6885	16.43673	25.10981	277.6043	23.02387	17.00222	194.4065	53.9862

Table 7. MATLAB data for ignited pellets (cont.)

30	40	29	10	28	27	26	19	6		
40	39	38	37	33	32	31	24	23		
21.88928	4.046151	3.012749	2.48676	6.751772	4.04633	4.698565	33.32435	19.848		
9.277493	12.47964	7.278462	5.704174	10.99103	11.66344	14.66638	1.008017	4.306783		
2.359396	0.32422	0.413927	0.435954	0.614298	0.346924	0.320363	33.0593	4.608545		
203.0777	50.49452	21.92818	14.18491	74.20893	47.19413	68.91097	33.59152	85.48104		
37.10937	18.2032	10.86092	13.27419	11.21436	10.45711	15.59202	34.73145	24.74867		
30.69722	31.01196	7.293192	5.756106	11.51909	13.12708	28.33584	1.358983	6.992797		
534.1771	437.5358	42.96519	27.69388	113.8393	112.5629	426.7513	45.11535	102.9989		
1213.898	475.4114	1039.444	73.5802	648.7693	231.9683	468.0791	8.828345	327.3689		
277.9273	158.2848	36.55358	18.71393	98.86882	63.85104	196.3682	25.92911	87.28906		

The real values for density and line resistance had some deviation from the target values. The lower density pellets are difficult to press in such a way that they hold together, and some of the 40% TMD target pellets ended up having higher densities (40.5% to 50.3%). The higher

density pellets were much closer to their targets. Line resistance values were different than their target values as well. The method of adjusting line resistance was connecting either of two specific resistors in line to the test circuit or not connecting one of them. For the target of 0.9 Ohms, the real line resistance ranged from 0.57 Ohms to 1.105 Ohms. One reason for this large range for this target, and the other line resistance targets, is that the clips used to attach to the heat pellet electrode wore out from mechanical strain and had to be replaced before the 31st test. For the 2.5 Ohm target, the range of real values was from 2.37 Ohms to 2.63 Ohms. For the 4 Ohm target, the range was from 3.87 Ohms to 4.05 Ohms.

To analyze the data, several software tools were used. The data recorded by the oscilloscope was processed by code written in MATLAB to compute power, energy, and resistance from the current and voltage data, as well as plotting the waveforms of each test. The statistical modeling and analysis tool JMP was used to evaluate the data.

An example of a standard waveform plot is shown below. The blue, red, and teal curves on the top plot correspond to voltage across the pellet, current measured by the CVR, and the light signal. The red square gives the time when the MATLAB code has detected the light out signal start to rise, which corresponds to the top of the pellet igniting. Dynamic resistance, power, and cumulative energy are derived from current, voltage, and time measurements.

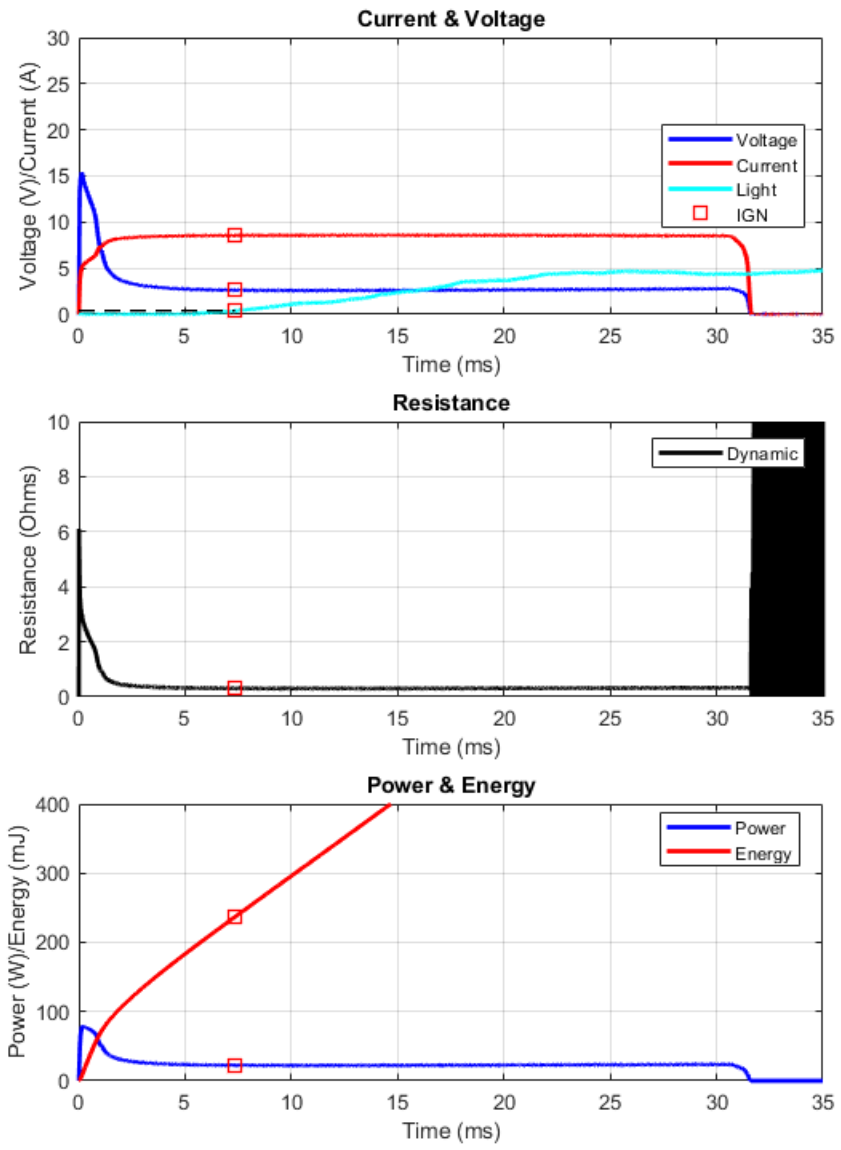

Figure 31. Example of a normal waveform – SN04, 88% Fe, sieved Fe, ball milled KClO4, 50% TMD, 0.020" gap, 100PSI, 36V, 4Ohm line resistance

Certain pellets had unique waveforms. Figure 32 shows an example of a "noisy" waveform. The exact reason for this phenomenon is not known, but it is theorized that poor contact between the electrodes and the iron network of heat pellet is the cause.

This affects the voltage and current data. Data that is derived from this is not accurate, which influences dynamic resistance, power, and energy calculations. However, since the fiber optic cable is not influenced by the same phenomenon, the light signal is not affected. Thus,

it can be used for determining the ignition time, even though the other electrical data collected from the oscilloscope presents a greater degree of uncertainty.

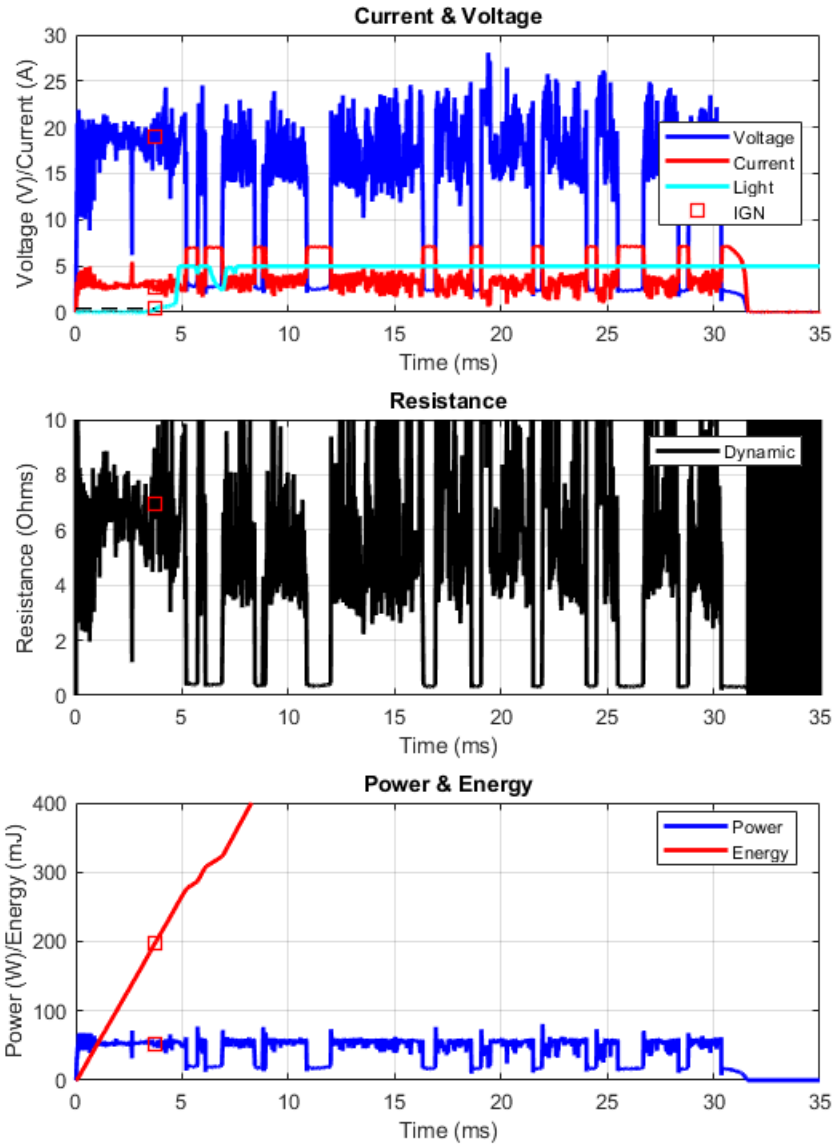

Figure 32. Example of a “noisy” waveform – SN04, 82% Fe, As Received Fe & KClO4, 40% TMD, 0.040” gap size, 100 PSI, 30V, 4 Ohm line resistance

Chapter 4. Results

4.1 Overview of Results

The goal of the testing and analysis was to confirm previously observed trends and to determine which variables are important for accurate characterization of performance. A secondary goal was to determine, if possible, which levels of the variables result in optimized performance. Therefore, the focus of this analysis is to obtain information about which variables have a statistically significant impact on the ignition response, and then find out which levels of those variables cause optimal responses. The optimal responses are pellet function ("go" instead of "no go"), low power and energy thresholds for ignition, and quick ignition response.

The variables analyzed in the study include the iron-potassium perchlorate ratio, iron particle size, potassium perchlorate particle size, pellet density measured during pressing, electrode gap size, the pressure applied to the pellet during testing, the measured line resistance of the ignition circuit, and the power supply voltage, as conveyed in Table 1. All these variables had targeted values for each sample, and efforts were made to get each sample as close to the test plan as possible.

4.2 Results

The first step of the analysis was to examine the relationship between the variables and the noisiness vs. smoothness of the waveforms, and then perform a similar analysis with the response being go vs. no go. After this, similar modeling was performed with ignition responses: time to ignition, cumulative energy, and average power. For the noise and result

responses, a nominal logistic fit was used. For ignition time, cumulative energy, and average power, a standard least squares fit was used.

4.2.1 Noise in Data - Response

The noise analysis revealed that density, pressure, iron content, and the electrode gap size were all important variables contributing to this phenomenon, and that other variables did not have an effect.

The first run of the model resulted in unstable parameter estimates and an R-squared value of one. This indicates that the model is perfectly predicting the response, or the data is too sparse. As seen by the JMP screenshot (Figure 33), the model suggests that density is what perfectly predicts the noisy response. When density is removed from the model, the order of the other variables changes. The R squared value also drops significantly, which again suggests that density is the main variable of significance.

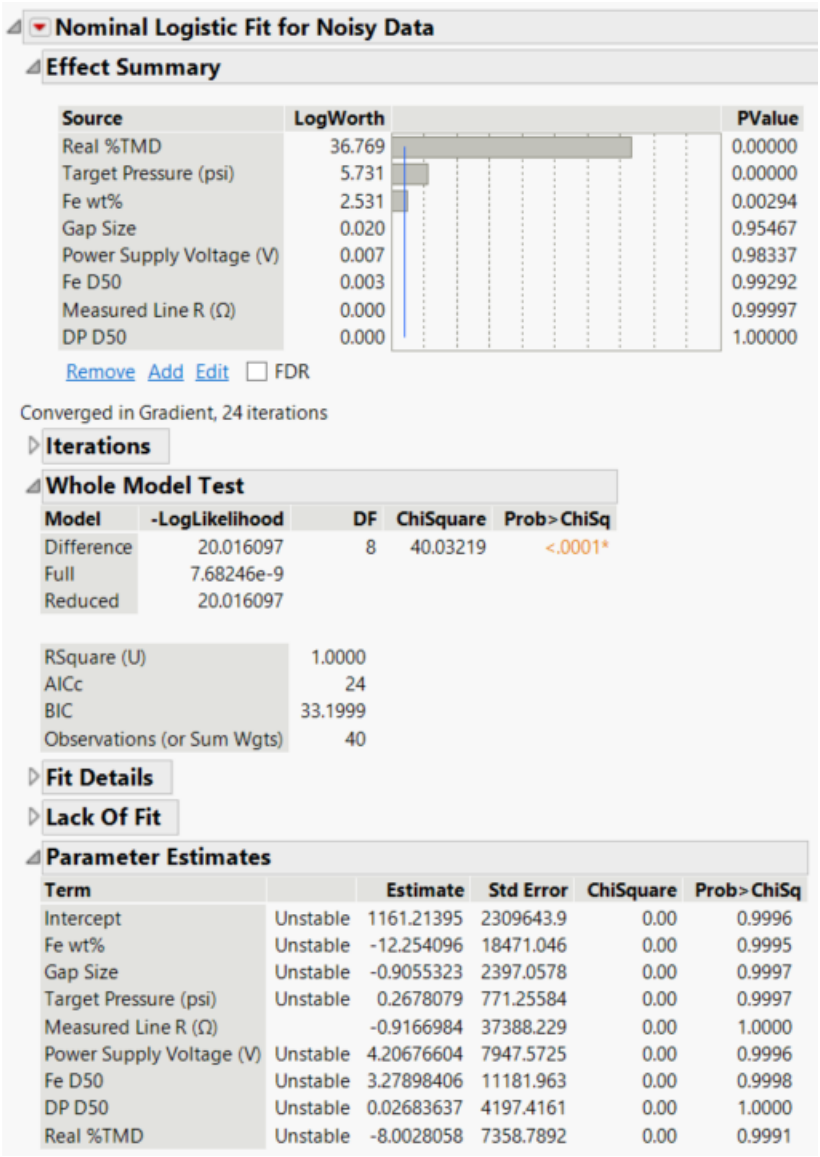

Nominal Logistic Fit for Noisy Data

Effect Summary

Source	LogWorth	PValue
Real %TMD	36.769	0.00000
Target Pressure (psi)	5.731	0.00000
Fe wt%	2.531	0.00294
Gap Size	0.020	0.95467
Power Supply Voltage (V)	0.007	0.98337
Fe D50	0.003	0.99292
Measured Line R (Ω)	0.000	0.99997
DP D50	0.000	1.00000

Remove Add Edit ☐ FDR

Converged in Gradient, 24 iterations

Iterations

Whole Model Test

Model	-LogLikelihood	DF	ChiSquare	Prob>ChiSq
Difference	20.016097	8	40.03219	<.0001*
Full	7.68246e-9			
Reduced	20.016097			

RSquare (U)	1.0000
AICc	24
BIC	33.1999
Observations (or Sum Wgts)	40

Fit Details

Lack Of Fit

Parameter Estimates

Term		Estimate	Std Error	ChiSquare	Prob>ChiSq
Intercept	Unstable	1161.21395	2309643.9	0.00	0.9996
Fe wt%	Unstable	-12.254096	18471.046	0.00	0.9995
Gap Size	Unstable	-0.9055323	2397.0578	0.00	0.9997
Target Pressure (psi)	Unstable	0.2678079	771.25584	0.00	0.9997
Measured Line R (Ω)		-0.9166984	37388.229	0.00	1.0000
Power Supply Voltage (V)	Unstable	4.20676604	7947.5725	0.00	0.9996
Fe D50	Unstable	3.27898406	11181.963	0.00	0.9998
DP D50	Unstable	0.02683637	4197.4161	0.00	1.0000
Real %TMD	Unstable	-8.0028058	7358.7892	0.00	0.9991

Figure 33. Summary of effects for noisy data model fit – including density

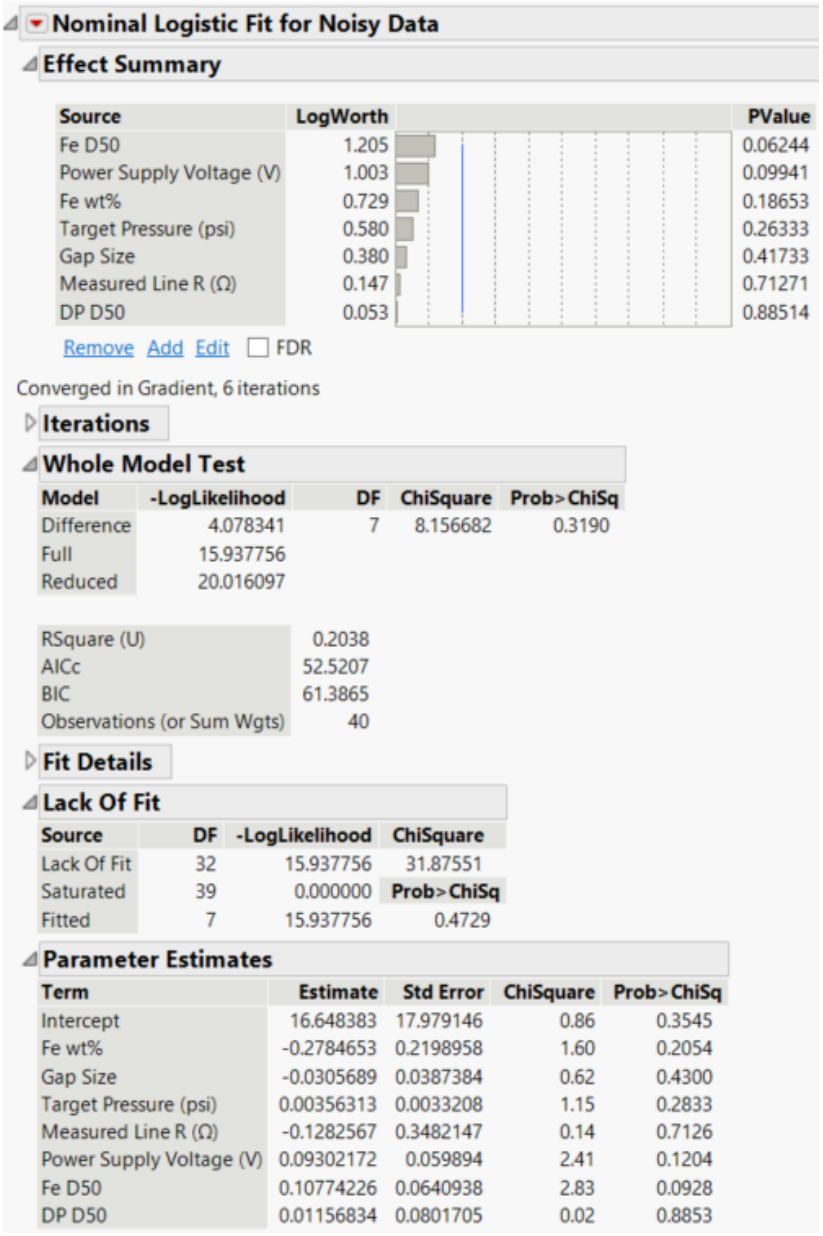

Nominal Logistic Fit for Noisy Data

Effect Summary

Source	LogWorth	PValue
Fe D50	1.205	0.06244
Power Supply Voltage (V)	1.003	0.09941
Fe wt%	0.729	0.18653
Target Pressure (psi)	0.580	0.26333
Gap Size	0.380	0.41733
Measured Line R (Ω)	0.147	0.71271
DP D50	0.053	0.88514

Remove Add Edit ☐ FDR

Converged in Gradient, 6 iterations

Iterations

Whole Model Test

Model	-LogLikelihood	DF	ChiSquare	Prob>ChiSq
Difference	4.078341	7	8.156682	0.3190
Full	15.937756			
Reduced	20.016097			

RSquare (U)	0.2038
AICc	52.5207
BIC	61.3865
Observations (or Sum Wgts)	40

Fit Details

Lack Of Fit

Source	DF	-LogLikelihood	ChiSquare
Lack Of Fit	32	15.937756	31.87551
Saturated	39	0.000000	Prob>ChiSq
Fitted	7	15.937756	0.4729

Parameter Estimates

Term	Estimate	Std Error	ChiSquare	Prob>ChiSq
Intercept	16.648383	17.979146	0.86	0.3545
Fe wt%	-0.2784653	0.2198958	1.60	0.2054
Gap Size	-0.0305689	0.0387384	0.62	0.4300
Target Pressure (psi)	0.00356313	0.0033208	1.15	0.2833
Measured Line R (Ω)	-0.1282567	0.3482147	0.14	0.7126
Power Supply Voltage (V)	0.09302172	0.059894	2.41	0.1204
Fe D50	0.10774226	0.0640938	2.83	0.0928
DP D50	0.01156834	0.0801705	0.02	0.8853

Figure 34. Summary of effects for noisy data model fit – without density

When running the analysis without density included, no variable was statistically significant ($p <= 0.05$). Iron particle size was close to significance, but it is clear that density is the main effect that causes this phenomenon. The noisiness in the waveforms was not present for the 60% or 70% TMD samples. It appears that there is a threshold somewhere between 50% and

60% TMD, below which this phenomenon is much more likely. The second density graph also shows the threshold may be around 3 grams/cc.

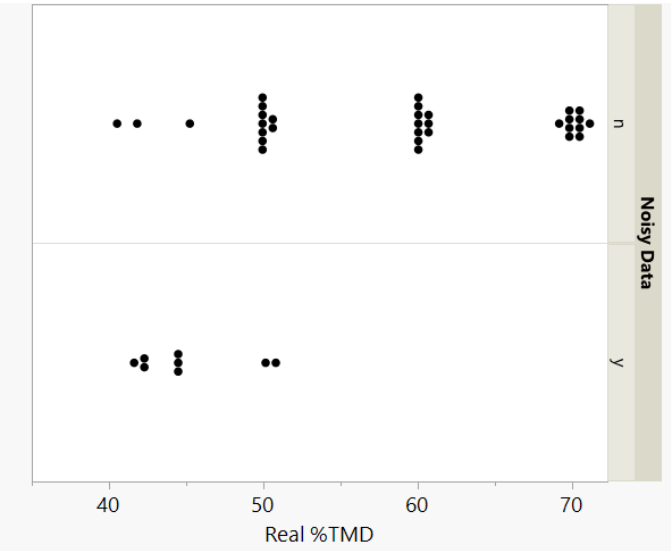

Figure 35. Noisy data level vs density (%TMD)

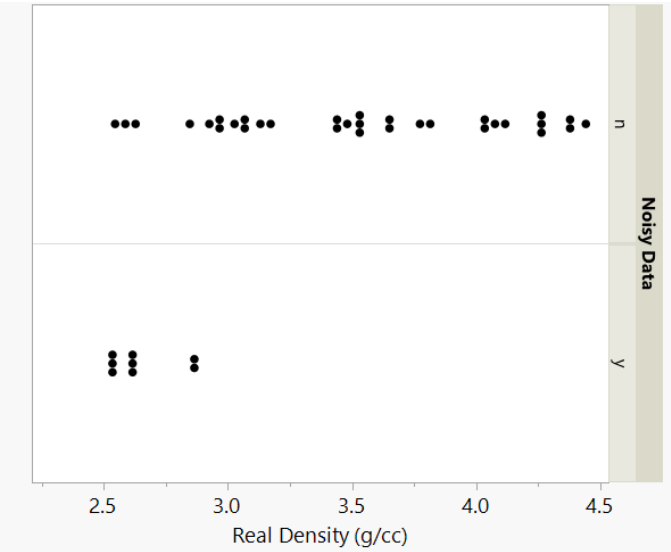

Figure 36. Noisy data level vs density (g/cc)

Running the model without density predicted that iron particle size and power supply voltage had some smaller effect ($p <= 0.1$). The next few graphs summarize these effects.

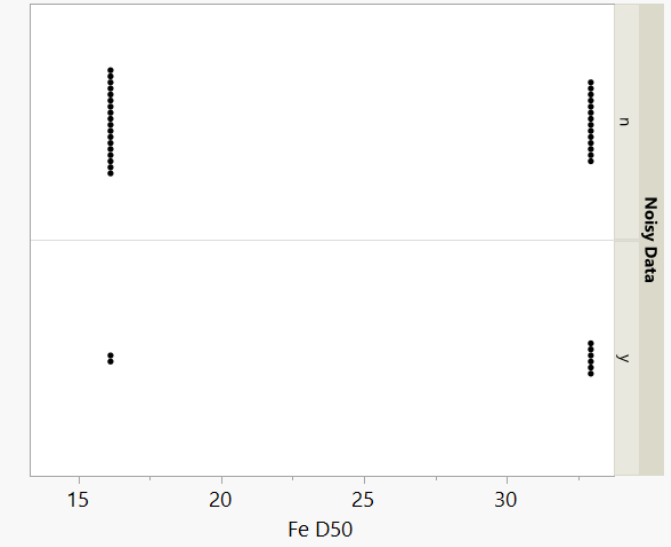

Figure 37. Noisy data level vs iron particle size

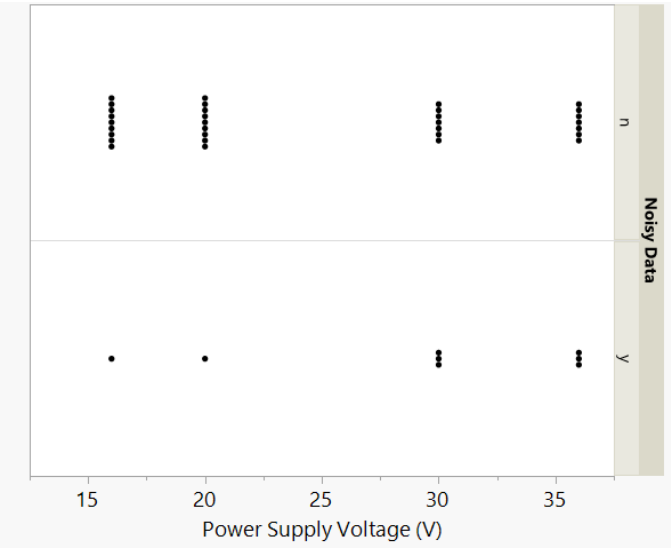

Figure 38. Noisy data level vs power supply voltage

4.2.2 Go/No Go Result - Response

The same model type was used to fit the data for the result (go/no go) response. Similarly to the analysis of the noisy data, running the nominal logistic fit model resulted in an R-squared value of 1, and unstable parameter estimates.

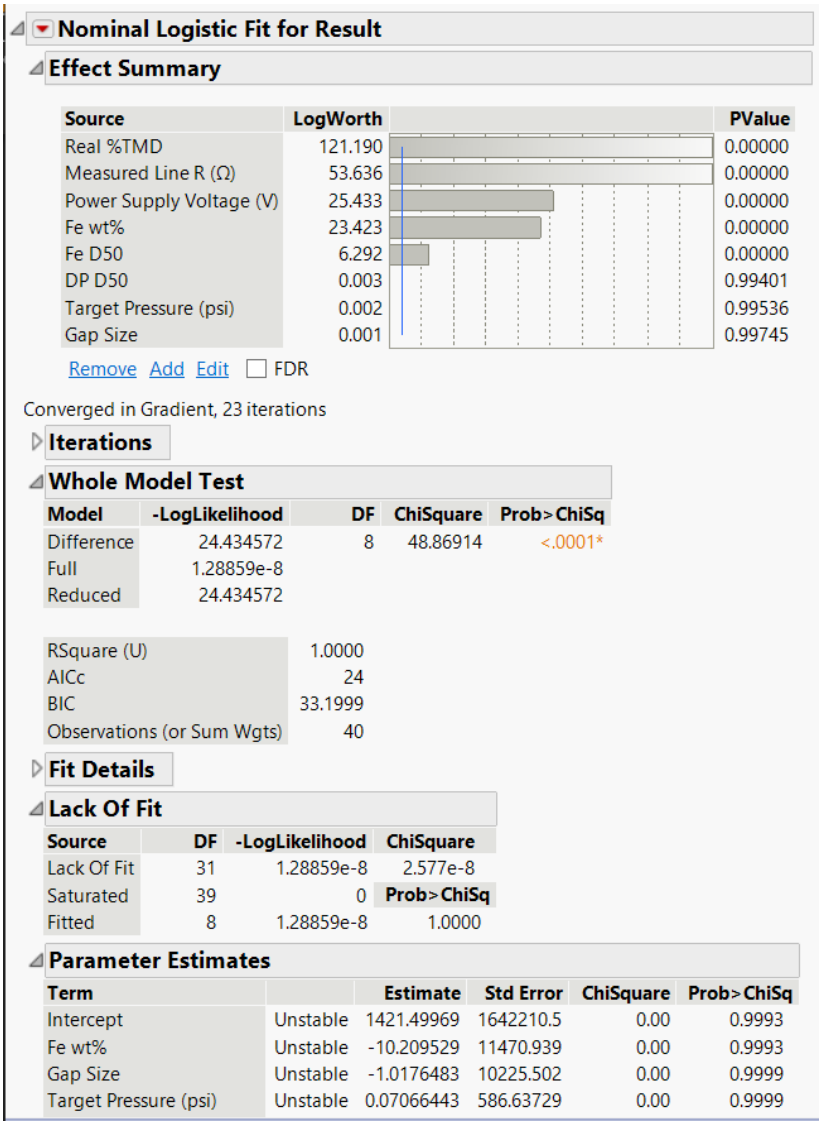

Nominal Logistic Fit for Result

Effect Summary

Source	LogWorth	PValue
Real %TMD	121.190	0.00000
Measured Line R (Ω)	53.636	0.00000
Power Supply Voltage (V)	25.433	0.00000
Fe wt%	23.423	0.00000
Fe D50	6.292	0.00000
DP D50	0.003	0.99401
Target Pressure (psi)	0.002	0.99536
Gap Size	0.001	0.99745

Remove Add Edit ☐ FDR

Converged in Gradient, 23 iterations

Iterations

Whole Model Test

Model	-LogLikelihood	DF	ChiSquare	Prob>ChiSq
Difference	24.434572	8	48.86914	<.0001*
Full	1.28859e-8			
Reduced	24.434572			

RSquare (U)	1.0000
AICc	24
BIC	33.1999
Observations (or Sum Wgts)	40

Fit Details

Lack Of Fit

Source	DF	-LogLikelihood	ChiSquare
Lack Of Fit	31	1.28859e-8	2.577e-8
Saturated	39	0	Prob>ChiSq
Fitted	8	1.28859e-8	1.0000

Parameter Estimates

Term		Estimate	Std Error	ChiSquare	Prob>ChiSq
Intercept	Unstable	1421.49969	1642210.5	0.00	0.9993
Fe wt%	Unstable	-10.209529	11470.939	0.00	0.9993
Gap Size	Unstable	-1.0176483	10225.502	0.00	0.9999
Target Pressure (psi)	Unstable	0.07066443	586.63729	0.00	0.9999

Figure 39. Summary of effects for test result model fit – unstable model

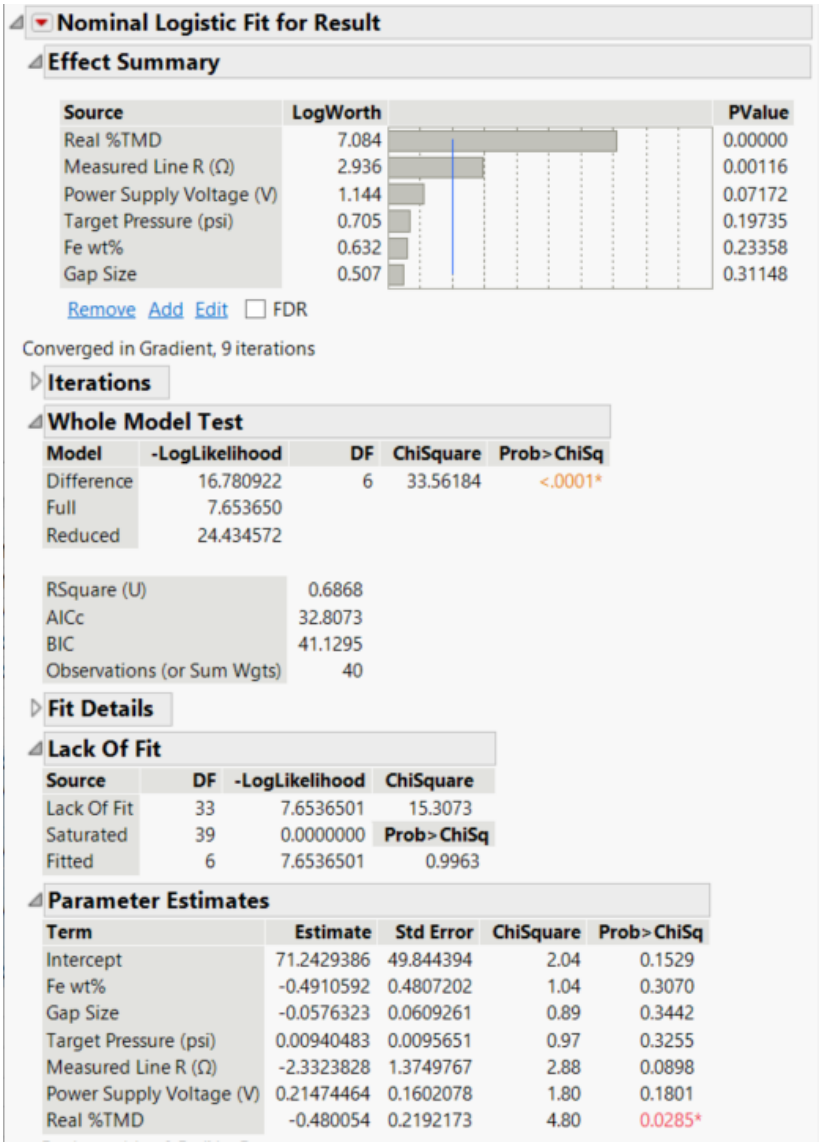

Nominal Logistic Fit for Result

Effect Summary

Source	LogWorth	PValue
Real %TMD	7.084	0.00000
Measured Line R (Ω)	2.936	0.00116
Power Supply Voltage (V)	1.144	0.07172
Target Pressure (psi)	0.705	0.19735
Fe wt%	0.632	0.23358
Gap Size	0.507	0.31148

Remove Add Edit ☐ FDR

Converged in Gradient, 9 iterations

Iterations

Whole Model Test

Model	-LogLikelihood	DF	ChiSquare	Prob>ChiSq
Difference	16.780922	6	33.56184	<.0001*
Full	7.653650			
Reduced	24.434572			

RSquare (U)	0.6868
AICc	32.8073
BIC	41.1295
Observations (or Sum Wgts)	40

Fit Details

Lack Of Fit

Source	DF	-LogLikelihood	ChiSquare
Lack Of Fit	33	7.6536501	15.3073
Saturated	39	0.0000000	Prob>ChiSq
Fitted	6	7.6536501	0.9963

Parameter Estimates

Term	Estimate	Std Error	ChiSquare	Prob>ChiSq
Intercept	71.2429386	49.844394	2.04	0.1529
Fe wt%	-0.4910592	0.4807202	1.04	0.3070
Gap Size	-0.0576323	0.0609261	0.89	0.3442
Target Pressure (psi)	0.00940483	0.0095651	0.97	0.3255
Measured Line R (Ω)	-2.3323828	1.3749767	2.88	0.0898
Power Supply Voltage (V)	0.21474464	0.1602078	1.80	0.1801
Real %TMD	-0.480054	0.2192173	4.80	0.0285*

Figure 40. Summary of effects for test result model fit – stable model

The parameters of the first model were unstable because the data was too separated, leading to the logistic fit not predicting the response correctly. Each particle size variable had two levels, which could cause this separation in the data. After removing both iron and potassium perchlorate particle size variables from the model, the parameters became stable, with an R-squared value of 0.6868. Again, density was a large factor, along with line resistance. Power supply voltage had a smaller effect. The rest of the variables are not considered important, except for particle size, which will be discussed later.

At 50% TMD and below, all pellets ignited. 70% TMD was somewhat less likely than 60% to ignite. With increasing line resistance, the likelihood of ignition decreased.

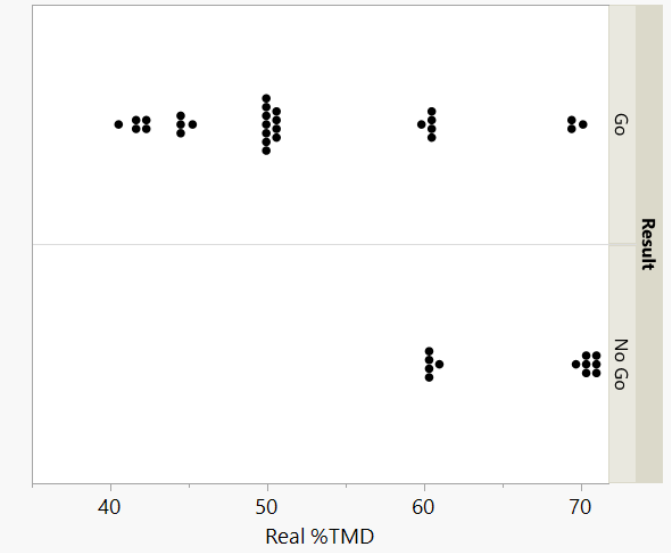

Figure 41. Result vs measured percentage of theoretical maximum density

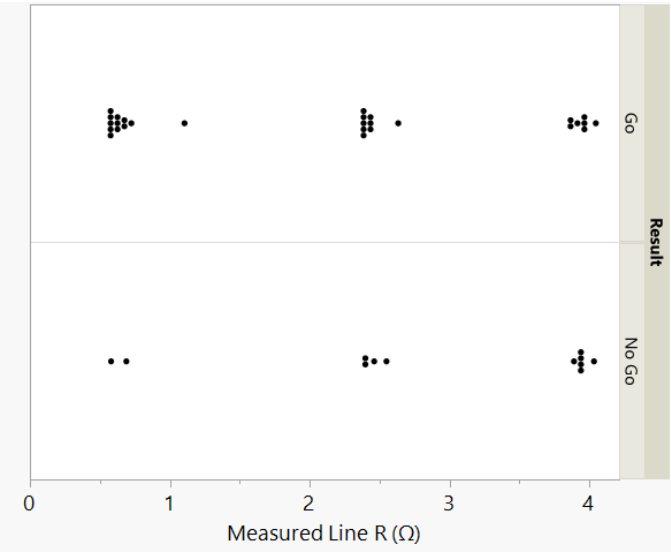

Figure 42. Result vs measured line resistance

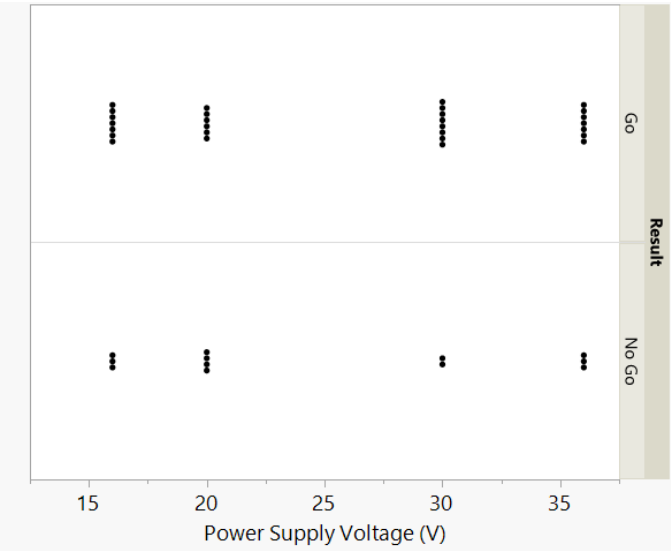

Figure 43. Result vs power supply voltage

Since particle size was removed from the model due to a too-great level of separation, a different analysis was performed to try to determine the level of importance. The following figure shows a contingency analysis indicating that smaller iron particle sizes (SV meaning sieved iron particles) have some effect, while smaller potassium perchlorate particle sizes do not. The statistical significance of this analysis is questionable, but the results appear to line up with observations from prior testing and literature.

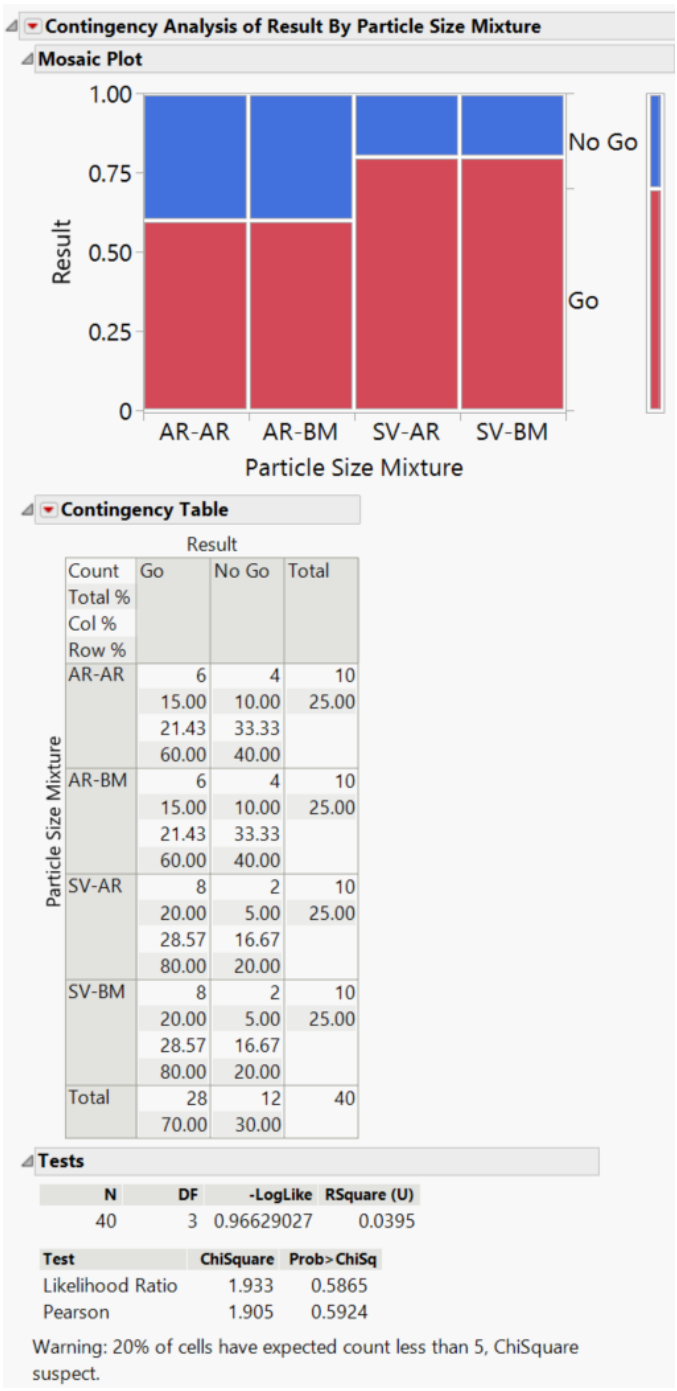

Figure 44. Contingency analysis of effect of particle size mixture on result

4.2.3 Ignition Time - Response

The next response to be considered is the time from the start of the ignition pulse to ignition. To determine the time of ignition, the MATLAB code determines when the voltage signal rises, which corresponds to light from the burning heat pellet reaching the light sensor. The algorithm used to determine this works by iterating through the light signal data and taking a window of data after each point. In the code used for these experiments, the 500^{th} point is where the iteration starts and the window is 200 points after. If the average of the window after the point is larger than the maximum of the signal data times a threshold (in this case 0.01), then the time at that point is considered to be the time of ignition. The light signal is not very noisy so this method is very accurate.

Only the "go" results are considered. Also important to note is that, because many of the higher density pellets did not ignite, the data for ignition time does not include those pellets. If the ignition pulse was longer, it is possible these pellets would have ignited. However, since ignition times under 10ms are preferred, the behavior of these pellets would not have been acceptable.

Effect Summary

Source	LogWorth	PValue
Gap Size	2.064	0.00863
Power Supply Voltage (V)	1.080	0.08326
Measured Line R (Ω)	0.939	0.11502
DP D50	0.553	0.27984
Fe wt%	0.548	0.28298
Real %TMD	0.489	0.32458
Fe D50	0.461	0.34568
Target Pressure (psi)	0.074	0.84300

Remove Add Edit ☐ FDR

Residual by Predicted Plot

Summary of Fit

RSquare	0.486904
RSquare Adj	0.270863
Root Mean Square Error	5.562398
Mean of Response	6.561429
Observations (or Sum Wgts)	28

Analysis of Variance

Source	DF	Sum of Squares	Mean Square	F Ratio
Model	8	557.8556	69.7320	2.2538
Error	19	587.8653	30.9403	Prob > F
C. Total	27	1145.7209		0.0698

Parameter Estimates

Term	Estimate	Std Error	t Ratio	Prob>|t|
Intercept	-52.62586	49.05927	-1.07	0.2968
Fe wt%	0.5941867	0.537754	1.10	0.2830
Fe D50	0.1272905	0.131631	0.97	0.3457
DP D50	-0.214715	0.193017	-1.11	0.2798
Real %TMD	0.1431564	0.141558	1.01	0.3246
Gap Size	0.2699474	0.092193	2.93	0.0086*
Target Pressure (psi)	-0.001494	0.007441	-0.20	0.8430
Measured Line R (Ω)	1.4427541	0.873484	1.65	0.1150
Power Supply Voltage (V)	-0.254222	0.139052	-1.83	0.0833

Figure 45. Summary of effects for ignition time

The most significant variable is the electrode gap size, followed by power supply voltage and line resistance.

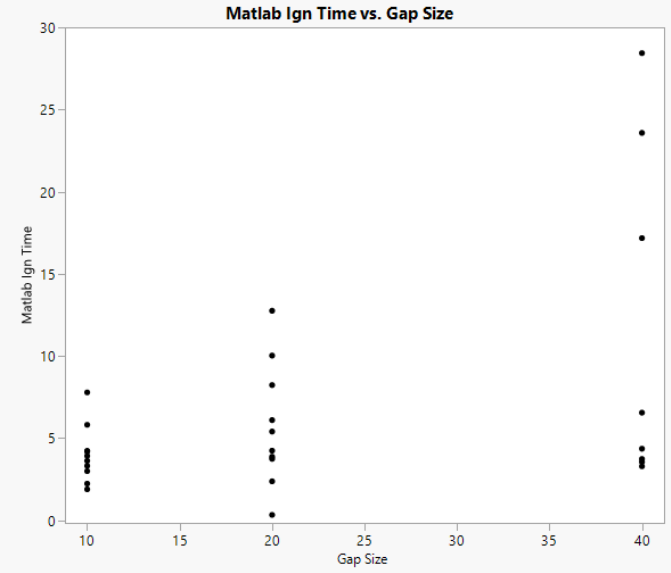

Figure 46. Time to ignition vs. gap size

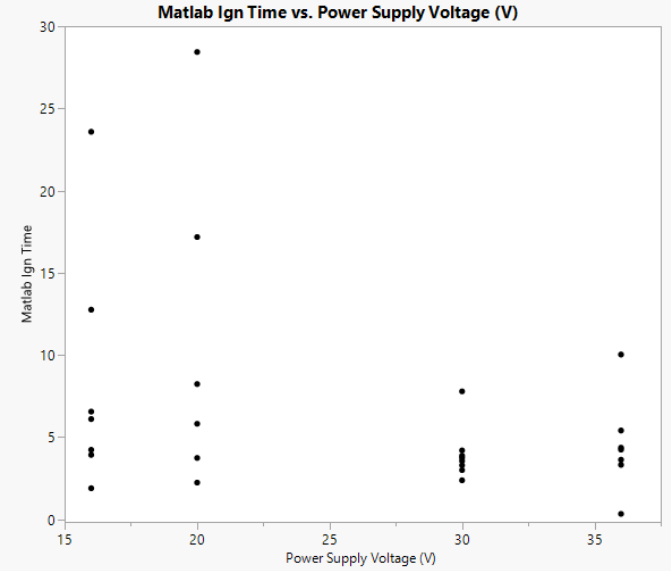

Figure 47. Time to ignition vs. power supply voltage

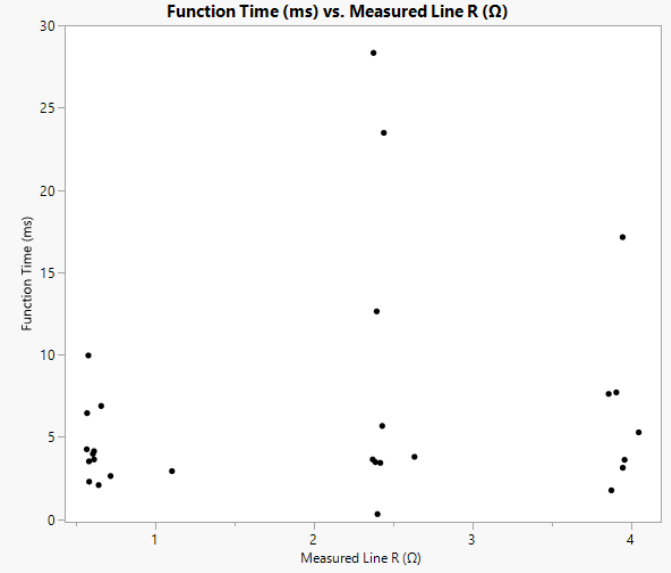

Figure 48. Time to ignition vs. line resistance

The smallest gap size produced more consistent and lower ignition times. While the median function time value remained similar, the maximum function times increased dramatically (Figure 49). Higher voltage also showed a trend towards faster and more consistent ignitions above 20 Volts (Figure 50).

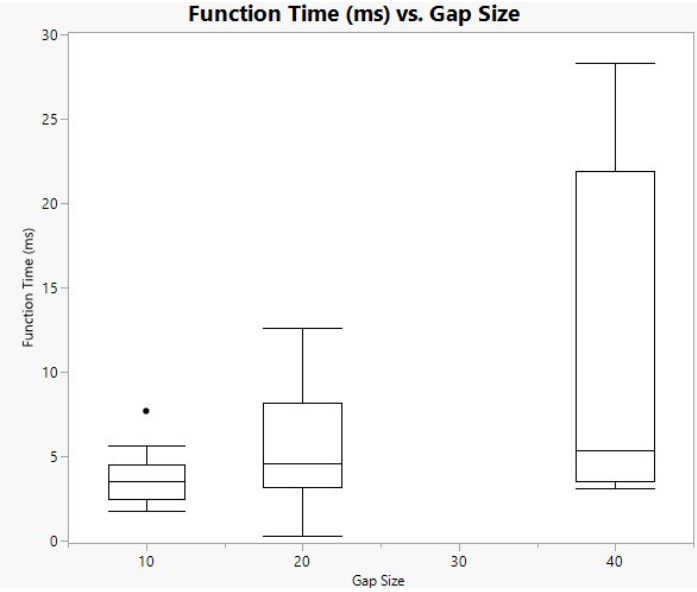

Figure 49. Box plot graph of function time vs gap size.

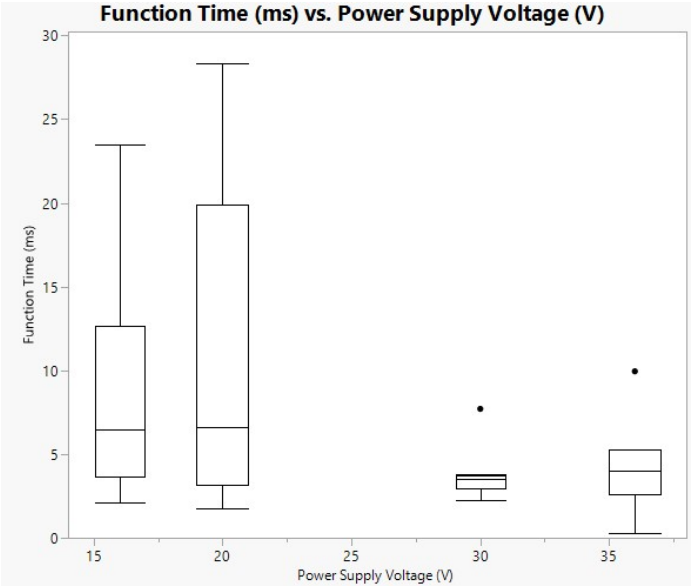

Figure 50. Box plot graph of function time vs power supply voltage

4.2.4 Average Power - Response

Average power is measured from the start of the signal to the ignition time. Again, the tests with noisy data and no goes were not included.

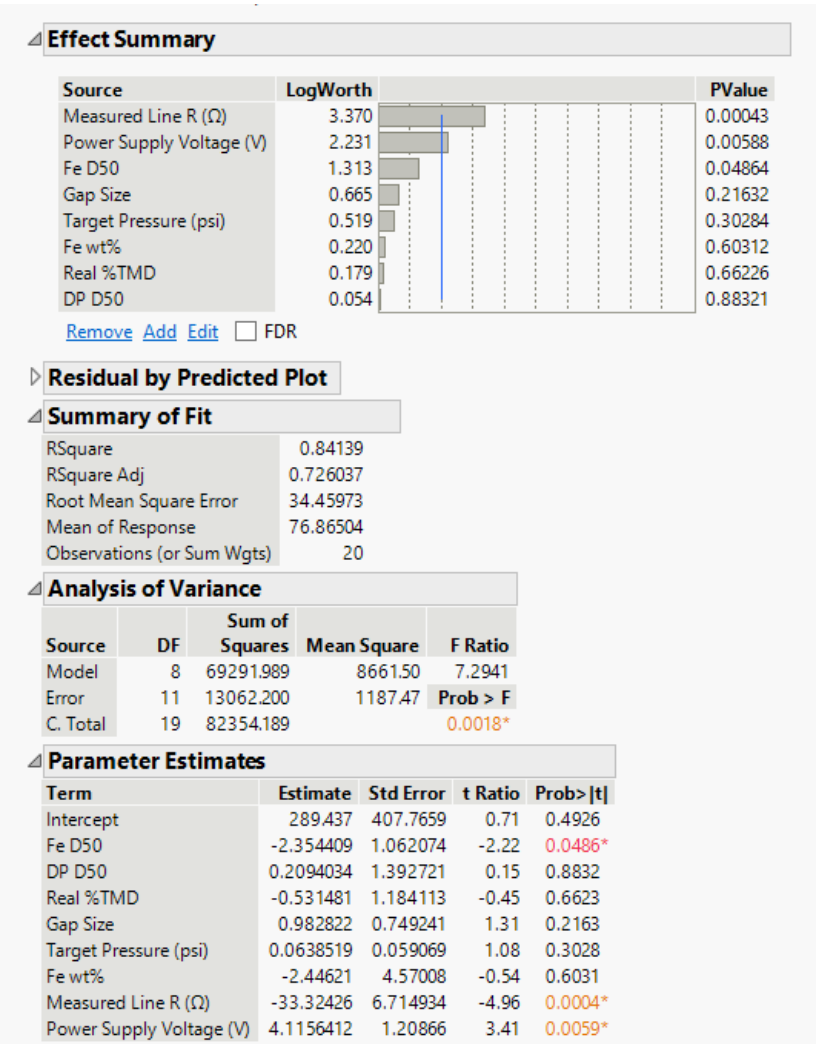

Effect Summary

Source	LogWorth	PValue
Measured Line R (Ω)	3.370	0.00043
Power Supply Voltage (V)	2.231	0.00588
Fe D50	1.313	0.04864
Gap Size	0.665	0.21632
Target Pressure (psi)	0.519	0.30284
Fe wt%	0.220	0.60312
Real %TMD	0.179	0.66226
DP D50	0.054	0.88321

Remove Add Edit ☐ FDR

Residual by Predicted Plot

Summary of Fit

RSquare	0.84139
RSquare Adj	0.726037
Root Mean Square Error	34.45973
Mean of Response	76.86504
Observations (or Sum Wgts)	20

Analysis of Variance

Source	DF	Sum of Squares	Mean Square	F Ratio
Model	8	69291.989	8661.50	7.2941
Error	11	13062.200	1187.47	Prob > F
C. Total	19	82354.189		0.0018*

Parameter Estimates

Term	Estimate	Std Error	t Ratio	Prob>|t|
Intercept	289.437	407.7659	0.71	0.4926
Fe D50	-2.354409	1.062074	-2.22	0.0486*
DP D50	0.2094034	1.392721	0.15	0.8832
Real %TMD	-0.531481	1.184113	-0.45	0.6623
Gap Size	0.982822	0.749241	1.31	0.2163
Target Pressure (psi)	0.0638519	0.059069	1.08	0.3028
Fe wt%	-2.44621	4.57008	-0.54	0.6031
Measured Line R (Ω)	-33.32426	6.714934	-4.96	0.0004*
Power Supply Voltage (V)	4.1156412	1.20866	3.41	0.0059*

Figure 51. Summary of effects for average power

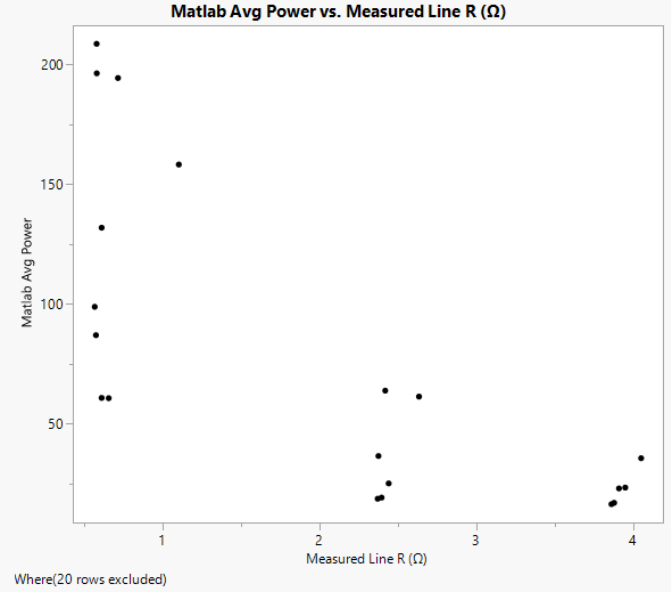

Figure 52. Average power vs measured line resistance

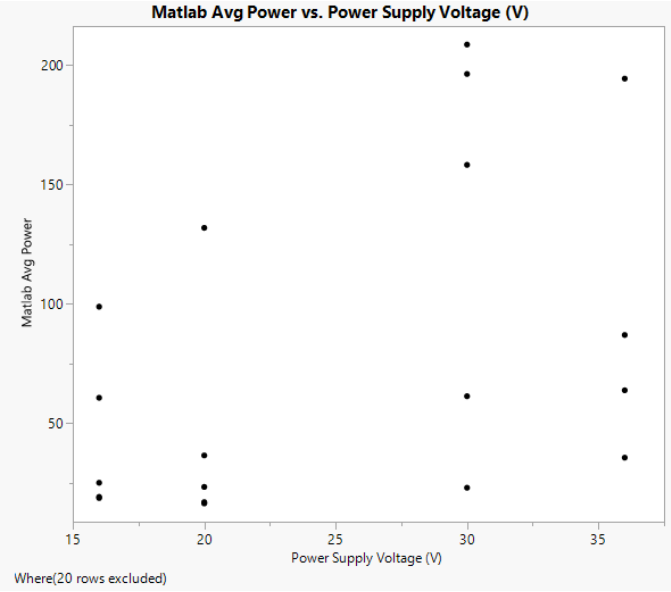

Figure 53. Average power vs power supply voltage

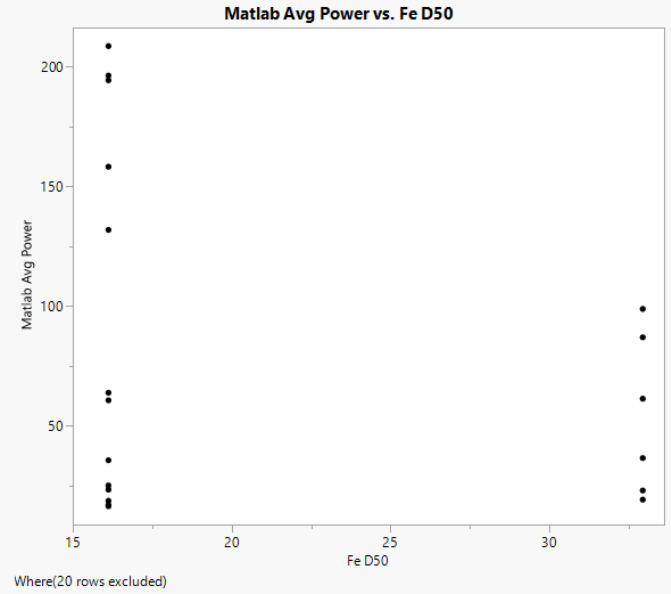

Figure 54. Average power vs iron particle size (50th percentile)

Line resistance and voltage were the most significant variable for average power, with iron particle size playing a lesser role. The decreasing and increasing trends for line resistance and voltage make sense when considered with the equation relating power to voltage and resistance, where P represents power, V voltage, and R resistance.

$$P = \frac{V^2}{R}$$

4.2.5 Cumulative Energy - Response

The next response to be looked at was cumulative energy at ignition. The results with noisy data are not included, as the voltage and current data that cumulative energy is calculated from is likely not measured correctly. Also, the no-go results are not included since the response depends on the time of ignition.

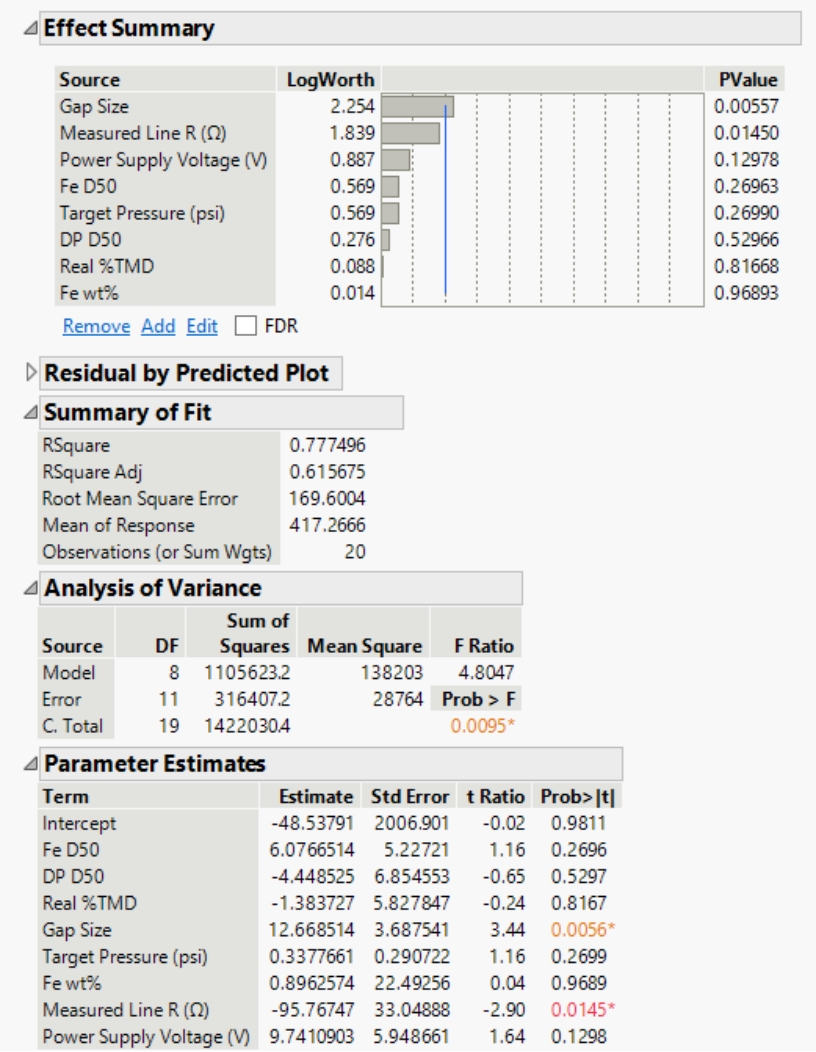

Effect Summary

Source	LogWorth	PValue
Gap Size	2.254	0.00557
Measured Line R (Ω)	1.839	0.01450
Power Supply Voltage (V)	0.887	0.12978
Fe D50	0.569	0.26963
Target Pressure (psi)	0.569	0.26990
DP D50	0.276	0.52966
Real %TMD	0.088	0.81668
Fe wt%	0.014	0.96893

Remove Add Edit ☐ FDR

Residual by Predicted Plot

Summary of Fit

RSquare	0.777496
RSquare Adj	0.615675
Root Mean Square Error	169.6004
Mean of Response	417.2666
Observations (or Sum Wgts)	20

Analysis of Variance

Source	DF	Sum of Squares	Mean Square	F Ratio
Model	8	1105623.2	138203	4.8047
Error	11	316407.2	28764	Prob > F
C. Total	19	1422030.4		0.0095*

Parameter Estimates

Term	Estimate	Std Error	t Ratio	Prob>|t|
Intercept	-48.53791	2006.901	-0.02	0.9811
Fe D50	6.0766514	5.22721	1.16	0.2696
DP D50	-4.448525	6.854553	-0.65	0.5297
Real %TMD	-1.383727	5.827847	-0.24	0.8167
Gap Size	12.668514	3.687541	3.44	0.0056*
Target Pressure (psi)	0.3377661	0.290722	1.16	0.2699
Fe wt%	0.8962574	22.49256	0.04	0.9689
Measured Line R (Ω)	-95.76747	33.04888	-2.90	0.0145*
Power Supply Voltage (V)	9.7410903	5.948661	1.64	0.1298

Figure 55. Summary of effects for cumulative energy response

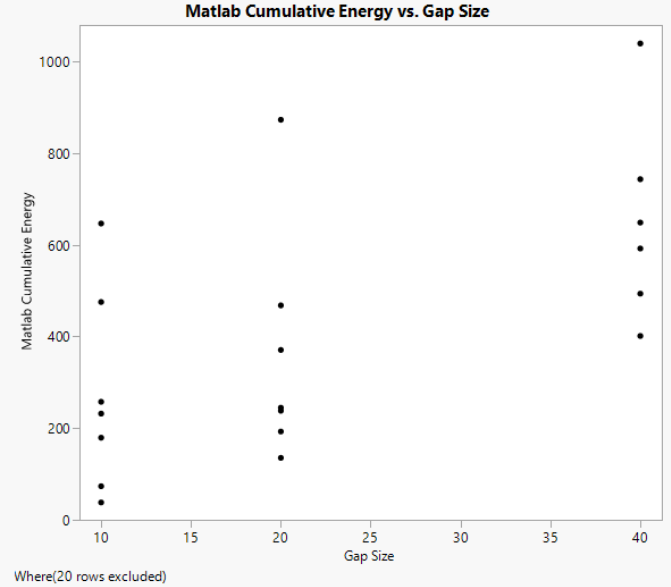

Figure 56. Cumulative energy vs. gap size

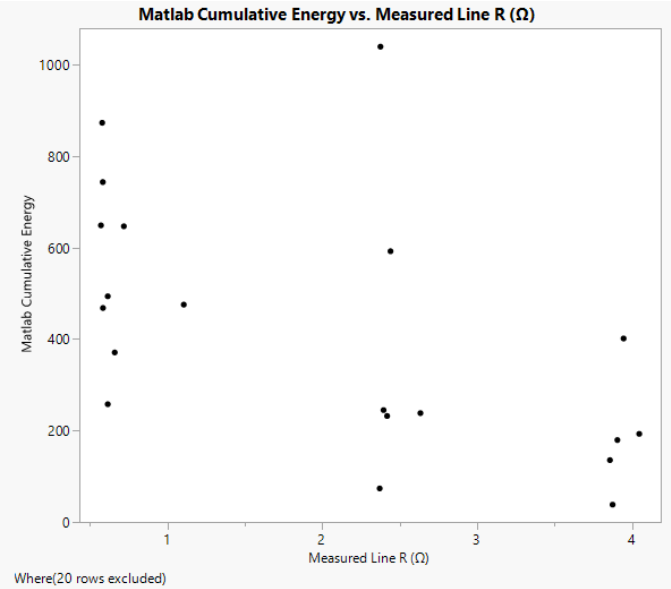

Figure 57. Cumulative energy vs. measured line resistance

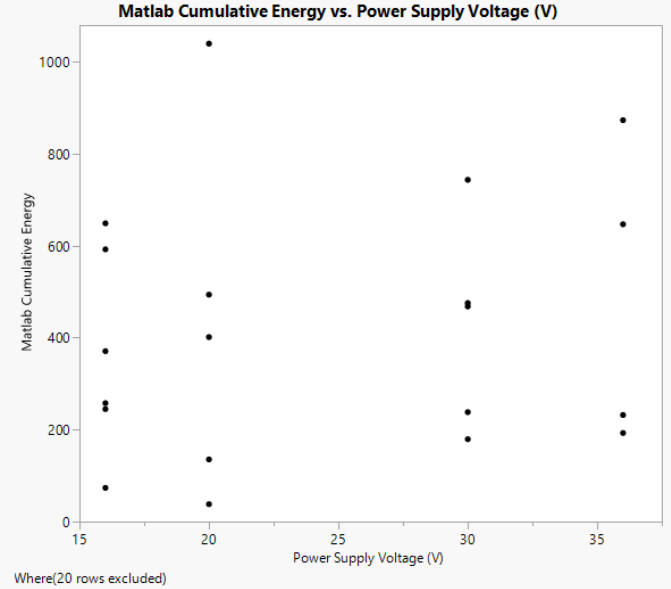

Figure 58. Cumulative energy vs. power supply voltage

The responses for gap size and line resistance show fairly clear trends, pointing to a lower gap size and higher line resistance for minimizing the cumulative energy.

Chapter 5. Discussion and Analysis

5.1 Ignition Result

It is critical that heat pellets work reliably in a thermal battery application. Therefore, the most important response is the ignition result. Density affected this response the most, so it is the most important variable. This conclusion is congruent in much of the prior work developing and characterizing heat pellets. Additionally, there was a clear correlation between increasing density and decreasing chance of ignition.

The density of the pellet affects heat and electrical conduction within the pellet. Particles that are pressed together more tightly will conduct better. This can be seen by examining the heat equation:

$$\frac{\partial T}{\partial t} = \frac{k}{\rho c_p} \nabla^2 T$$

Where T is temperature, t is time, k is thermal conductivity, c_p is specific heat capacity, and ρ is density of the material. All else being equal, a higher material density means slower heat transfer. However, since heat pellets are not solid, porosity is extremely important. Therefore, k will need to be calculated for the case of powders. While this is a very complicated subject, especially for two-phase powders, the Maxwell-Eucken model (Xue, 1991) can be used to gain some idea of how k changes with porosity:

$$k = k_s \frac{1 - (1 - \left(3 \frac{k_s}{2k_s + k_a}\right) \frac{k_a}{k_s}) \varphi}{1 + (3 \frac{k_s}{2k_s + k_a} - 1) \varphi}$$

Where k is thermal conductivity of the powder, k_s is thermal conductivity of the solid, k_a is thermal conductivity of air, and φ is porosity. If k_a is assumed to be much smaller than k_s, then the equation simplifies to:

$$k = k_s \frac{1}{1 + 0.5\varphi}$$

As pressing density increases, porosity decreases, and thus the value of k increases. With an increase in thermal conductivity, the heat transfer rate must also increase.

For resistive activation, better conduction can be undesirable for two reasons: low electrical resistance does not generate as much heat when fixed voltage is applied, and low heat resistance allows heat to leave the volume between the electrodes more quickly. Both of these factors lead to lower temperatures between the electrodes during the ignition pulse, and therefore a lower chance of ignition.

Line resistance was of secondary importance to the ignition result response. To get the maximum power dissipated in the heat pellet, the pellet resistance should match the line resistance as closely as possible, according to Jacobi's law, which states that maximum power transfer from a source to a load will occur when the resistance of the source is the same as the resistance of the load. The dynamic resistance of the pellet tends to drop lower than one Ohm after a few milliseconds, and it is likely that this is fairly close to the lower line resistance values.

Iron particle size also appears to have an effect, but due to problems running the model, the relative importance to the other factors in this study is difficult to ascertain. However,

previous testing and literature points to particle size as an important variable, so it is worthy of future consideration.

Particle size is likely to be of importance to ignition because the combustion reaction will start more quickly with smaller particles. This is because the particles will have greater contact area when at least one material is of lower size. From the screening study experiments, it does not appear that smaller potassium perchlorate particles affect ignition, and the reason for this is unclear. Rittenhouse (1970) showed that smaller potassium perchlorate did lead to improved likelihood of ignition, so further investigation may be necessary to explain the discrepancy between these different results.

5.2 Noisy Data

Noisiness in the data is not an important response for pellet performance, but it is interesting to know why it happens. Density was the only really significant factor, with densities below 50% TMD or 3 g/cc producing this response. As seen in the graphs above, lower densities are better for ignition performance, and reducing noisiness of the data is a much lower priority than obtaining better ignition characteristics. Therefore, while it is good to know what influences this response, it does not influence the final choice of optimal pellet parameters.

5.3 Ignition Time

The next response to be considered is ignition time. For use in thermal batteries, this is the second most important response, as these batteries are required to respond quickly to an ignition signal. Gap size was the most significant variable, followed by voltage and line resistance.

The gap sizes in this study were smaller than previously considered in the 2020 study (Padilla, 2020), where the gap sizes were larger (0.04”, 0.08”, and 0.12”). In that work, cumulative energy results were more favorable for smaller spacings but showed little difference for ignition time and average power.

The importance of gap size to ignition time in this work could be attributed to the smaller range of sizes, or the differences in the testing setups. The current theoretical understanding of resistive ignition mechanics suggests that a smaller gap size should result in faster ignition, since there is less volume of material that heat is dispersed into. Differences in gap size could also change the resistance of the pellet, but no correlation was found between pellet resistance and gap size. This is true for both dynamic resistance as calculated from the waveforms (excluding noisy data), and loaded pre-test resistance as measured by the resistance tester.

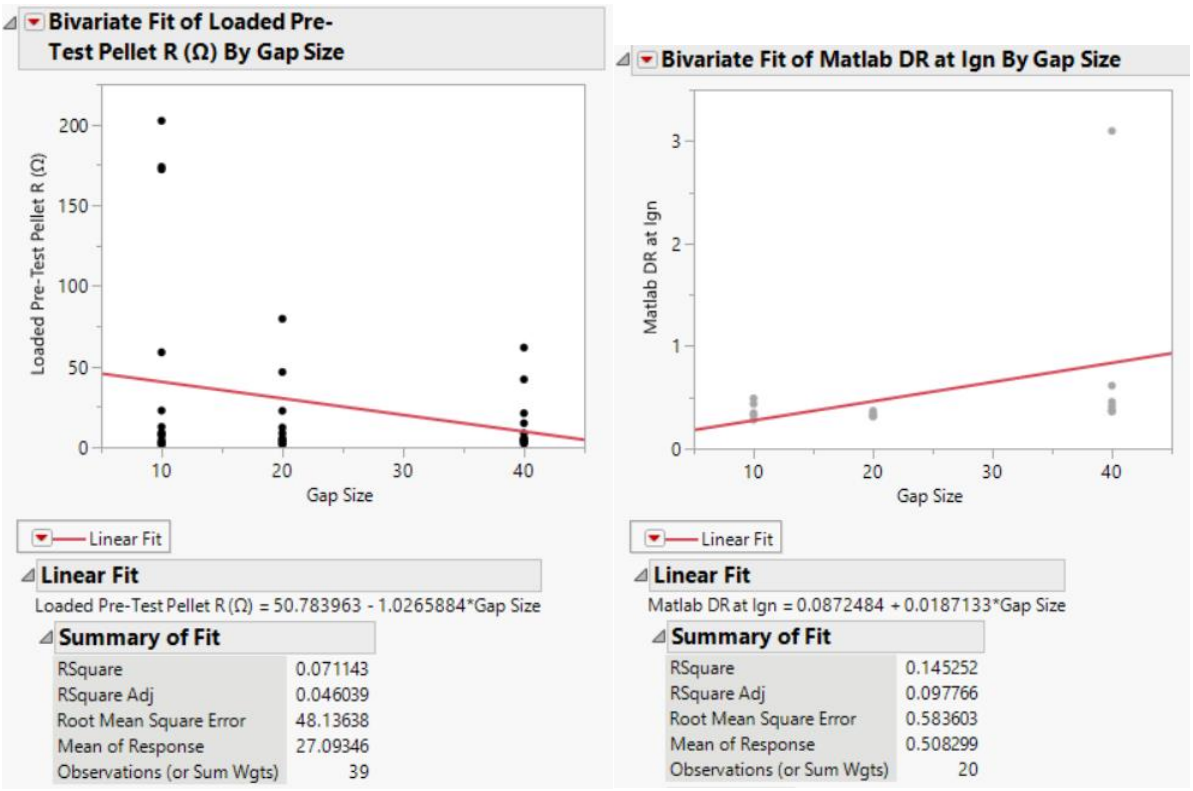

Figure 59. Loaded pre-test pellet resistance and dynamic resistance vs. gap size

Voltage and line resistance determine the amount of power the pellet receives. These, however, are not as easily controlled as the other variables since they are determined by the system design. From a battery design perspective, the greater significance of gap size is ideal.

5.4 Average Power

Minimizing average power required for ignition is an important consideration as well. As expected, line resistance and power supply voltage had the greatest effect. Iron particle size had a much smaller, but still statistically significant effect. Larger iron particle sizes resulted in lower power needed for ignition. The reason for this is unclear, but it is possible that

differences in heat conduction between different particle size mixtures affect how quickly the resistive heat dissipates into the pellet.

5.5 Cumulative Energy

Similarly to the 2020 study, gap size is a major contributor to the variability in cumulative energy at ignition. It is the most important factor, followed by line resistance. Cumulative energy could be understood as being very closely related to the product of ignition time and average power. Therefore, it is not surprising to see that the most important factors for those responses are also important for cumulative energy.

5.6 Summary of Findings

Overall, the goals of the experiment were met. The significant factors were identified, and some design parameters for ideal ignition were found. In rough order of importance, the most important parameters were pellet density, gap size, line resistance, iron particle size, and power supply voltage. This also revealed that the difference between the levels of pressure and the iron-potassium perchlorate ratios examined in this experiment are not significant. As mentioned before, iron-potassium perchlorate ratios below 80% are not practical for thermal battery application, and higher ratios are not commonly used in thermal batteries. Some previous studies showed that the ratio mattered to ignition, but their test setups were much different.

Optimum levels were identified to achieve a quick ignition with low power. Lower density pellets, smaller gap sizes, lower line resistance, and higher voltages will optimize ignition. All of these factors besides line resistance and voltage are easily changed for a thermal battery design. Line resistance and voltage are determined by the design of the greater system

that thermal batteries are used in. Line resistance is more likely to be flexible than voltage for future system designs, and since line resistance is more significant to ignition responses, this is a promising result.

There was variability in the models that was not accounted for. As mentioned before, the contact area of the electrodes was controlled by laser welder ablation, which is done by hand. This resulted in visual differences between electrodes used in testing, and this may correspond to differing contact areas between electrodes. This could explain the variability in pre-test loaded resistance and could be a major factor in the unexplained variability in ignition responses. New electrode designs in development at the time of writing are flexible printed circuit electrodes with exposed copper pads, which have well-controlled contact areas. This will likely lead to decreased variability in resistance measurements and ignition responses.

Chapter 6. Conclusions

Resistive activation developed as a response to the desire for a new method of reliably activating thermal batteries. Replacing igniters and heat paper would improve manufacturability and may improve reliability.

To progress the goal of reliable thermal battery activation, work has been done to develop electrode and heat pellet design. Before designing this experiment, some prior experiments were done to move towards ideal designs. However, since there are many factors involved in heat pellet design, until now no screening study had been performed in the context of resistive activation.

The experiment described in this work was successful in its goal of determining the relative importance of each factor. Additionally, ideal levels of several factors were identified to further refine the design of heat pellets.

The main factors identified were pellet density, electrode gap size, circuit line resistance, power supply voltage, and iron particle size. Density and gap size especially stood out among the other factors with large changes in the responses. Density, gap size, and iron particle size are fairly easy variables to change, but line resistance and voltage are controlled by the design of the larger system. Nevertheless, this information is evidence that could lead to change of design for a future iteration of the system.

The electrode setup for future resistive activation experiments is likely to change to a flexible printed circuit design. Despite this, the conclusions from this work will still apply to this design, as the activation mechanism is similar. As a result of this work, the design space is

better understood and will serve to support the development of this technology into production thermal batteries.

List of References

1

Guidotti, R. A., & Masset, P. (2006). Thermally activated ("thermal") battery technology. *Journal of Power Sources, 161*(2), 1443–1449. https://doi.org/10.1016/j.jpowsour.2006.06.013

2

Niu, Y., Wu, Z., Du, J., & Duan, W. (2014). A new thermal battery for powering borehole equipment: The discharge performance of Li–Mg–B alloy/LiNO3–KNO3/MnO2 cells at high temperatures. *Journal of Power Sources*, *245,* 537-542. https://doi.org/10.1016/j.jpowsour.2013.06.140

3

Guidotti, R. A. (1995). *Thermal batteries: A technology review and future directions. (Sandia Report)* SAND -95-1313C. Sandia National Lab. (SNL-NM), Albuquerque, NM (United States).

4

Rittenhouse, C. T. (1970). inal report on the development of pelletized heat sources for thermal batteries (No. SC-CR-70-6137). Unidynamics, Phoenix, Ariz..

5

Klasons, V., & Lamb, C. M. (2002). Chapter 21: Thermal Batteries. In D. Linden & T. B. Reddy (Eds.), *Handbook of Batteries* (3rd ed., pp. 21.1-21.6). McGraw-Hill.

6

Guidotti, R. A., Odinek, J., & Reinhardt, F. W. (2006). Characterization of Fe/KClO4 heat powders and pellets. *Journal of Energetic Materials*, *24*(4), 271-305.

7

Padilla, H. A. (2020). *Bridgeless Ignition of Thermal Battery Heat Pellets. (Sandia Report)* SAND2020-11754R. Sandia National Lab. (SNL-NM), Albuquerque, NM (United States).

8

JMP [Computer Software]. (2021) Retrieved from https://www.jmp.com/en_us/home.html

9

Guidotti, R. A., Reinhardt, F. W., & Odinek, J. (2002). Characterization of Fe/KClO4 heat powders for thermal batteries. In *Proc. 29th Intern. Pyrotechnics Seminar* (Vol. 847).

10

Evans, T. P. (1984*). Ignition Sensitivity Testing: A Preliminary Approach. GEND Technical Memorandum* GEPP-TM-814.

11

Cooper, M. A., Erikson, W. W., & Oliver, M. S. (2021). Electrical conductivity of porous binary powder mixtures. *Mechanics of Materials*, *162*, 104026.

12

Abdelmoneim, H. (2010). Dielectric and AC Conductivity of Potassium Perchlorate, KCLO_4. *Acta Physica Polonica A*, *117*(6), 936-940.

13

Lee, J., Yun, T. S., & Choi, S. U. (2015). The effect of particle size on thermal conduction in granular mixtures. *Materials*, *8*(7), 3975-3991.

14

Reinholz, E. L., & Wesolowski, D. E. (2014). Manufacturing and Temperature Effects on Heat Pellet Ignition Sensitivity (No. SAND2014-2938C). Sandia National Lab. (SNL-NM), Albuquerque, NM (United States).

15

Béquin, P., & Tournat, V. (2010). Electrical conduction and Joule effect in one-dimensional chains of metallic beads: hysteresis under cycling DC currents and influence of electromagnetic pulses. *Granular Matter*, 12, 375-385.

16

Leheup, E. R., & Moon, J. R. (1978). Electrical conductivity changes during compaction of pure iron powder. *Powder Metallurgy*, *21*(4), 195-198.

17

McCarthy, D. K., Leslie, W. B., & Dietzel, R. W. (1985). *Burn front velocity as a function of pellet density in iron/potassium perchlorate heat powders (Sandia Report)* SAND-83-1025. Sandia National Lab. (SNL-NM), Albuquerque, NM (United States).

18

Xue, S. S., & Barlow, J. W. (1991) Models for the Prediction of the Thermal Conductivities of Powders. *1991 International Solid Freeform Fabrication Symposium.* The University of Texas at Austin. https://repositories.lib.utexas.edu/handle/2152/64283?show=full